MARINE CLOUD BRIGHTENING

Authors:- John Latham[1,4] , Keith Bower[4] , Tom Choularton[4] , Hugh Coe[4], Paul Connelly[4] , Gary Cooper[7] ,Tim Craft[4], Jack Foster[7], Alan Gadian[5], Lee Galbraith[7] Hector Iacovides[4] , David Johnston[7] , Brian Launder[4], Brian Leslie[7] , John Meyer[7], Armand Neukermans[7], Bob Ormond[7], Ben Parkes[5] , Phillip Rasch[3], John Rush[7], Stephen Salter[6], Tom Stevenson[6], Hailong Wang[3], Qin Wang[7] & Rob Wood[2] .

Affiliations:- [1] National Centre for Atmospheric Research, Boulder, CO. [2] U Washington, Seattle, [3] PNNL, Richland, WA., [4] U Manchester, [5] U of Leeds, [6] U of Edinburgh, [7] Silver Lining, CA.

Abstract

The idea behind the marine cloud brightening (MCB) geoengineering technique is that seeding marine stratocumulus clouds with copious quantities of roughly monodisperse sub-micrometre seawater particles could significantly enhance the cloud droplet number concentration thus increasing the cloud albedo and longevity – thereby producing a cooling, which computations suggest could be adequate to balance the warming associated with a doubling of atmospheric carbon dioxide.

We review herein recent research on a number of critical issues associated with MCB: (1) general circulation model (GCM) studies, which are our primary tools to evaluate globally the effectiveness of marine cloud brightening and to assess its climate impacts on rainfall amounts and distribution, as well as on polar sea-ice cover and thickness: (2) high resolution modeling of the effects of seeding on marine stratocumulus, which are required to understand the complex array of interacting cloud processes involved in brightening: (3) microphysical modelling sensitivity studies examining the influence of seeding amount, seed-particle salt-mass, air-mass characteristics, updraught speed and other parameters on cloud-albedo change: (4) sea-water spray production by controlled electrohydrodynamic instability, and by microfabrication lithography: (5) computational fluid dynamics studies of possible large-scale periodicities in Flettner rotors: and (6) the planning of a three-stage limited-area field research experiment, which has the objective of developing our fundamental knowledge of marine stratocumulus clouds, testing the technology developed for the MCB geoengineering application, and ultimately, if deemed justifiable, field-testing the idea quantitatively, on a limited (perhaps 100km) spatial scale.

KEYWORDS: cloud brightening: albedo: GCM and high resolution modeling: cloud seeding: spray technology: field experiment

1.. Introduction

Cloud-brightening, one of several Solar Radiation Management (SRM) geoengineering ideas involving the production of a global cooling to compensate for the warming associated with continuing fossil fuel burning, was first postulated by Latham (1990, 2002). The ideas, engineering requirements, and climate impacts associated with cloud brightening have been significantly explored by Bower et al. (2006), Salter et al. (2008), Latham et al. (2008) and Rasch et al. (2009), Jones et al. (2009, 2010), Korhonen et al. (2010) , Bala et al. (2010) and Wang et al (2010).

The basic principle behind the idea is to seed marine stratocumulus clouds with seawater aerosol generated at or near the ocean surface. These particles would have sufficiently large salt-mass to ensure their subsequent growth within the clouds without being so large as to encourage precipitation formation, and would be sufficiently numerous to enhance the cloud droplet number concentration to values substantially higher than the natural ones, thereby enhancing the cloud albedo (Twomey, 1977). Enhancing the droplet concentration is likely also to affect the cloud macrophysical properties such as cloud cover, longevity, liquid water content and thickness, as a consequence of inhibiting precipitation formation (e.g. Albrecht 1989) and the timescale for the evaporation and sedimentation of cloud droplets.These feedbacks on the cloud properties can result in secondary aerosol indirect effects that are poorly understood and represent a major challenge in the general problem of understanding and quantifying how aerosols impact the climate system (Lohmann and Feichter 2005, Stevens and Feingold 2009, IPCC 2000).

Climate model simulations suggest that if the droplet concentration in marine stratocumulus can be increased to several hundred droplets per cm3 in a significant fraction of the stratocumulus sheets, then, in principle, a negative forcing can be produced, sufficient to offset doubled CO2 and maintain the polar sea-ice coverage at roughly current values. If this was achieved, the global distributions of surface temperature and sea-ice cover would inevitably be different from the present situation. Also, as demonstrated by the computations of Rasch et al (2009), the negative forcing required to hold the Earth's average surface temperature at the current value (in the face of CO2-doubling) would be different from that required for average sea-ice coverage maintenance (which would in fact be different at the two poles).

The principal objectives of this paper are to assess the current state of all significant aspects of recent work that we and others have conducted on MCB, to identify the major unresolved problems, and to outline our plans for further development of our work in these most important areas. We also hope to make it clear that the effective further development of our geoengineering study requires a comprehensive programme of fundamental research in several arenas, especially cloud physics.

The change in cloud albedo resulting from seeding the clouds with seawater particles large enough to be activated is roughly proportional to ln(N/No) (Twomey, 1977), where No and N are respectively the background droplet number concentration (prior to seeding) and the post-seeding value. No is therefore a critical parameter in determining the albedo enhancement resulting from seeding, so it is crucial to obtain accurate values of it, over the oceans. Recent observational work by Bennartz (2007), and Wood et al (2010), based on data from the NASA MODIS satellite instrument and airborne measurements in the VOCALS field experiment, are beginning to provide a reliable global assessment of No that has not been evaluated hitherto. These findings are illustrated in Figure 1.

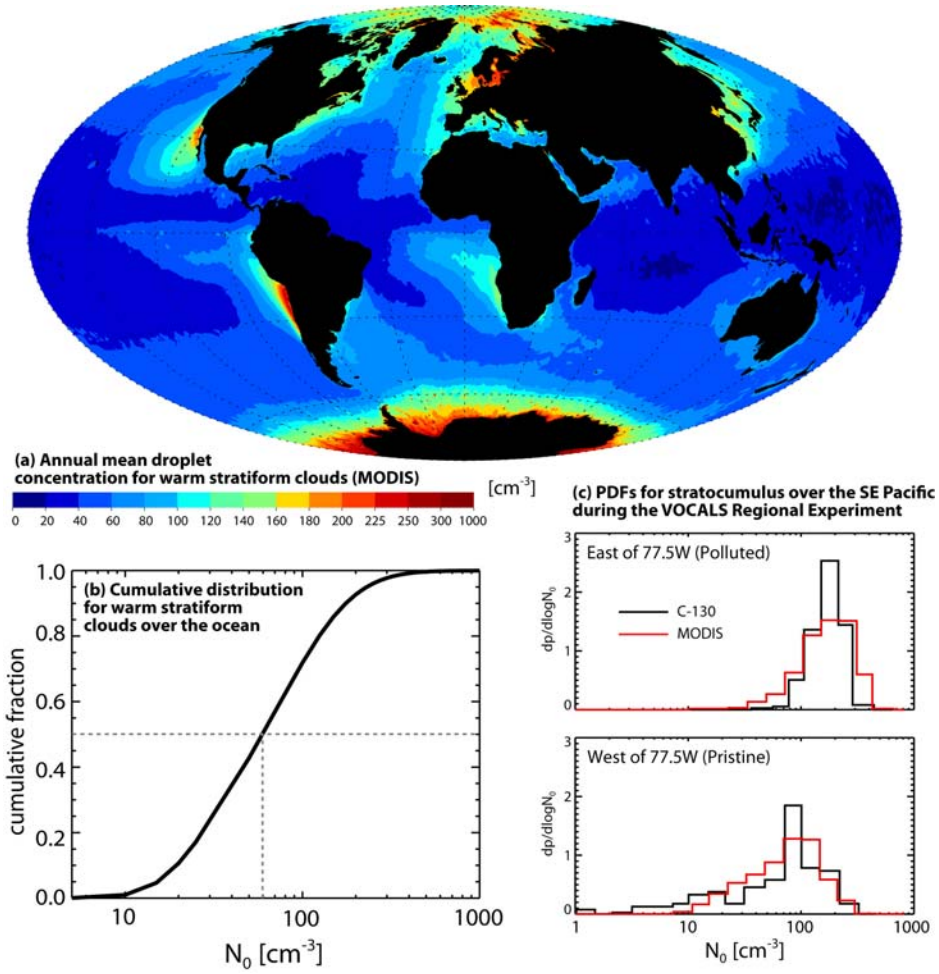

Figure 1. *Panel (a): Map of MODIS-derived annual mean cloud droplet concentration N_0 for stratiform marine warm clouds. To be included in the annual mean, the daily warm cloud fraction in 1x1 degree boxes must exceed 50% to capture primarily marine stratocumulus clouds. Panel (b): Cumulative distribution of daily 1x1 degree droplet number, N_0 from MODIS for all ocean points. Panel (c): Comparison of MODIS and C-130 aircraft measured cloud droplet concentration estimates from the VOCALS Regional Experiment during October/November 2008 off the Chilean coast (Wood et al. 2010), for longitudes 70-77.5°W (more polluted) and 77.5-85°W (more pristine). There is good agreement between in-situ and satellite-derived values which lends weight to the use of these data over the global oceans.*

The sections into which the paper is divided are: (a) GCM modeling of the cloud brightening scheme, and its influence on rainfall amounts and distributions, as well as sea-ice cover and thickness: (b) parcel modelling and its technological applications, (c) high-resolution cloud modelling: (d), spray production technologies under current investigation and Flettner rotor CFD modelling: (e), planning of a limited-area field research experiment, which has the objectives of developing our fundamental knowledge of marine stratocumulus clouds, and testing both MCB and the technology developed for this geoengineering application: (f) discussion.

2. Global Climate Modelling: Precipitation and Ice cover.

The objective of this section is to use the UK Met Office climate model, HadGEM1, (Hadley Centre Global Environmental Model) to study some climatological impacts of changing the cloud condensation nucleus (CCN) concentration in defined maritime oceanic regions which have

significant stratocumulus sheets. We present studies of the influence of this seeding on global precipitation and polar sea ice extent and thickness. There have been several GCM studies of MCB since the first atmosphere-only simulations, Latham et al., 2008). HadGAM, an atmosphere only climate model, has the advantage of an immediate response to greenhouse gas forcing, and can provide an immediate change in the Top of Atmosphere (TOA) radiative forcing. It is limited by having no component of ocean meridional heat transport flux and circulation. Slab GCM's have the advantage that short time scale thermocline changes are simulated. This can be suitable for NWP purposes, but is of limited representativity in climate studies. Fully coupled ocean-atmosphere GCM's include the large scale oceanic meridional heat transport, but the long time-constant ocean circulations provide the challenge of large scale hysteresis for the climate system. Jones et al (2009, 2010) used the UK Met Office HadGAM and HadGEM1 models. Bala et al (2010) and Rasch et al (2009) used the NCAR Community Climate System Model. In section 2.1, changes in precipitation resulting from seeding are discussed. In section 2.2, new results are presented on its impacts on ice thickness and ice extent.

The HadGEM1 model employed in our current studies is based on version 6.1 UK Met Office Unified Model (UM), with an atmospheric resolution of 1.25 by 1.875 degrees with 38 vertical levels, an upper lid at 39 km, and a coupled ocean model of variable grid size from 1 degree squares at the poles to 1/3rd of a degree at the Equator and to a depth of 5.3km using 40 levels. An emphasis in these models is on the improvement in the cloud and stratocumulus mixing parameterisations and this has been particularly useful in MCB studies, enabling improved calculations to be made of cloud droplet effective radius, radiative forcing and liquid water path (Martin et al. 2006). They have also provided the ability to focus on precipitation, surface temperature, cloud and sea surface temperatures, ice fraction and depth. HadGEM1 was used in the IPCC 2007 report (IPCC Working Group 1, 2007). The A1B case, is a standard scenario where technological developments are "balanced" and defined as not relying too heavily on fossil or non-fossil energy sources and also based on the assumption that similar improvement rates apply to both energy supply and end-use technologies.

With one exception, the results from previous simulations, and our own, show a significant increase in albedo in a seeded climate environment equivalent to compensating for an approximate doubling of planetary atmospheric CO_2. For the atmosphere only HadGAM computations, the equivalent TOA negative forcing is about -3.7 W/m^2 . The computations of Korhonen et al. (2010) predict smaller values of albedo-change and associated negative forcing but this is probably due to the fact that they used values of No which were between 2 and 3 times higher than the experimentally determined values for unpolluted regions presented in Figure 1**.** Simple calculations using the Twomey equations confirm that if their values of No are reduced by a factor of 2 or 3, the resulting values of negative forcing are roughly consistent with those of other workers.

In our study, three simulations were completed, each for 70 years from 2020 to 2090, with the last 20 years analysed; a control run with static carbon dioxide at 2020 levels (435ppm), a run with increasing carbon dioxide by 1%/year up to double pre-industrial carbon dioxide levels (560ppm at 2045).Case A was the control based on current (2020) carbon dioxide levels (435ppm).Case B was the control run plus 1% CO_2 increase p.a., until double pre-industrial levels (560 ppm) were reached, at which point the CO_2 levels were held static. Case C was as B, but with seeding of N=375cm^{-3} in three limited regions, off the Western coasts of California, Peru and Namibia, which Jones et al. (2009) highlighted as being particularly effective, due to their propensity for stratocumulus cloud fields in our current climatology.

2.1. Precipitation

The recent results from climate simulations cited above have shown variations in modelled precipitation when cloud seeding schemes have been introduced. The discussion here will focus on why this occurs, how these model results differ, and their significance.

Precipitation is not well described in climate models. The CPC Merged Analysis of Precipitation (CMAP) dataset provided by NOAA (Xie & Arkin, 1997) for 1979-2000 was compared with a ten year simulation using current static carbon dioxide levels. Figure 2a shows the difference between precipitation rate in HadGEM1 and the CMAP data set. The globally averaged difference in precipitation rates over land is 0.17 mm/day. Across most of the Northern land masses the precipitation difference is less than 1 mm/day. In the tropical regions the model does not well reproduce measured values downwind of particularly the South East Asian and South American mountain ranges. Across the globe the model is weakest in the presence of steep mountain ranges, on the West of a continental region. The increased precipitation on the upwind steep slopes produces an impact on the availability of water vapour in the lee of the mountains. It is within these limitations that results regarding precipitation patterns in a future seeded or non-seeded climate should be considered.

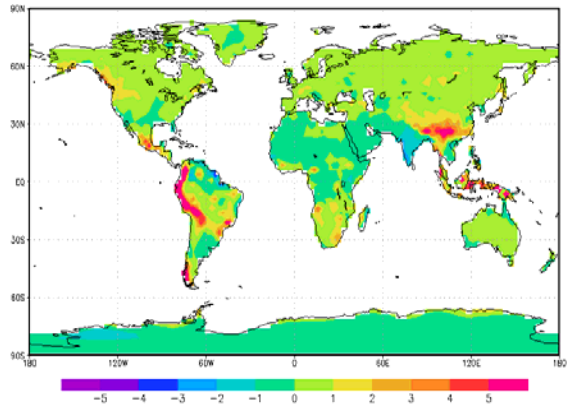

Figure 2a. *Difference in precipitation between CMAP and HadGEM1 simulations for current climate conditions. The units are mm/day. The global difference over land is 0.17mm/day. There are discrepancies in modelled precipitation in some tropical regions and near steep orography.*

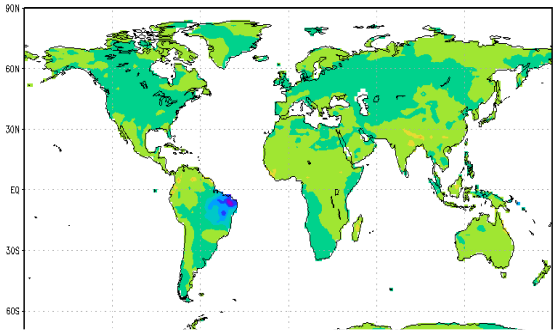

Figure 2(b). *Difference in precipitation resulting from simulations C – A (seeding of the three regions of stratocumulus - with current conditions). Units are mm/day. This plot shows the precipitation differences that could occur in a geoengineered scenario*

The difference in precipitation between simulations for seeded and control state A1B, CO2 simulations (C and A), Figure 2(b), is similar to Figure 4(b) in Jones et al (2009), Figure 3(b) in Rasch et al (2009) and Figure 7 in Bala et al (2010). Although each model has used a different seeding strategy, there is some degree of overlap. In cases where the whole maritime cloud has been seeded, the results do not on average differ significantly. Of course, this may be a function of the fact that climate models can have similar rainfall parameterisation schemes, but alternatively it may represent a realistic feature. The reduction of precipitation in Figure 2(b) for the whole averaged Amazon basin is consistent with that of Jones et al. (2009, 2010), but the decrease is much smaller in magnitude. However, for the whole of this region, the rainfall reduction is about the same as the errors in current model simulations compared with CMAP data, Figure 2(a), and is a result of the unrealistically large precipitation values in the desert area West of the Andes. Thus, the Jones et al (2010) results should be treated with caution in this region. Excess precipitation on upwind steep slopes removes downwind available atmospheric water vapour. This reduction is not present in Rasch et al (2009), but they seed a much larger portion of the ocean. The results of Bala et al. (2010), who seeded all suitable clouds, exhibit no significant Amazonian rainfall reduction, and globally indicate a small increase in precipitation over land. We note that our Case C simulation shows a relative increase in precipitation across sub-Saharan Africa and India. African and Indonesian precipitation increases are present in Rasch et al (2009). Bala et al (2010) find no significant reduction in precipitation in any land region. Recent results of Jones et al (personal communication), have indicated that their reduction in rainfall in the Amazon

region is a consequence of their seeding of the Southern Hemisphere stratocumulus cloud region, but the reason for this is not clear.

To summarise, one of the most difficult challenges in climate modelling is to predict more accurately global precipitation patterns. Our results show a small increase in precipitation in the dryer regions of Africa as indicated in Figure 2(b), with a small average decrease in the Amazon region. These results from our model indicate that there are changes in precipitation produced in the seeding cases, but that the variations are within the bounds of current model precision and uncertainties. Higher resolution and more accurate simulations are clearly required for future work.

2.2.. Sea Ice Extent and Thickness

The three maritime regions were seeded in a similar pattern to Jones et al. (2009, 2010). Figures 3 and 4 show the change in the summer minimum sea ice fraction and sea ice thickness respectively. The Arctic ice minimum has been taken to occur in September and the Antarctic minimum in March. All data has been taken from the final 20 years of the 70 years simulations.

Figures 3(a) and 3(b) show the significant reduction in sea ice fraction under a doubling of pre-industrial carbon dioxide atmosphere, Case B. There is a general and significant loss of sea ice in Polar regions. In the Southern Hemisphere, Figures 3(b) and 3(d) the reduction in sea ice is non-uniform, with the most significant reduction to be found East of the Antarctic Peninsula. The Arctic ice minimum in the double CO_2 scenario, Figure 3(a), Case B – Case A, is a 76% reduction from the 2020 ice extent, but with seeding switched on, Figure 3(c), Case C – Case A, the reduction is only 3%. In the Southern Hemisphere, Figures 3(b) and 3(d), the equivalent reductions are 30% and 17%.

In contrast, with the above, the sea ice depth increases close to the North Pole, Figures 4(a) and 4(c) creating a small central region of thicker ice in the double CO_2 scenario, and to a much lesser extent in the seeded scenario. This corresponds to a model increase in precipitation in this polar region. In the Southern ocean the changes are non-uniform and - in some existing ice regions - there is an increase in the South Polar minima sea ice thickness.

There are several major regions where the sea ice thickness is reduced by more than 2m, Figure 4(b), and again a lesser extent in the geoengineered case Figure 4(d). This is consistent with a southward movement of mid latitude weather patterns. The representation of the melt rate of glaciers is of concern since the current climate models seem unable to represent the observed more rapid change. It is therefore likely that the loss of ice may occur at a greater rate than current model predictions, 30% as cited above, for the double CO_2 scenario. With seeding on, at the North Pole, there remains an increase in sea ice thickness at the North Pole, but a marginal change at the South Pole.

In summary, taking both the ice fraction and depth characteristics together, seeding significantly reduces the sea ice fraction loss during the summer months. The Southern minima reduction in sea ice fraction is smaller than in the Northern Hemisphere. The increase in sea ice thickness near the pole in the geoengineered scenario does not alter the albedo of that region. Further, not shown here, there is a possible feedback effect which has not been included in the modelling. In the Northern Hemisphere Case C, there is an increase in sea ice fraction to the North of Siberia which increases the albedo relative to the control. The changes in ice cover fraction are consistent with those of Rasch et al (2009), but the reduction of the Southern Hemisphere ice fraction is smaller in our calculations. The simulations indicate that our seeding with $N=375cm^{-3}$, increases ice extent in the double CO_2 scenario. Results from seeding all the oceans, not presented here, produces a further enhancement of planetary albedo and growth of polar ice cover compared with the control scenario.

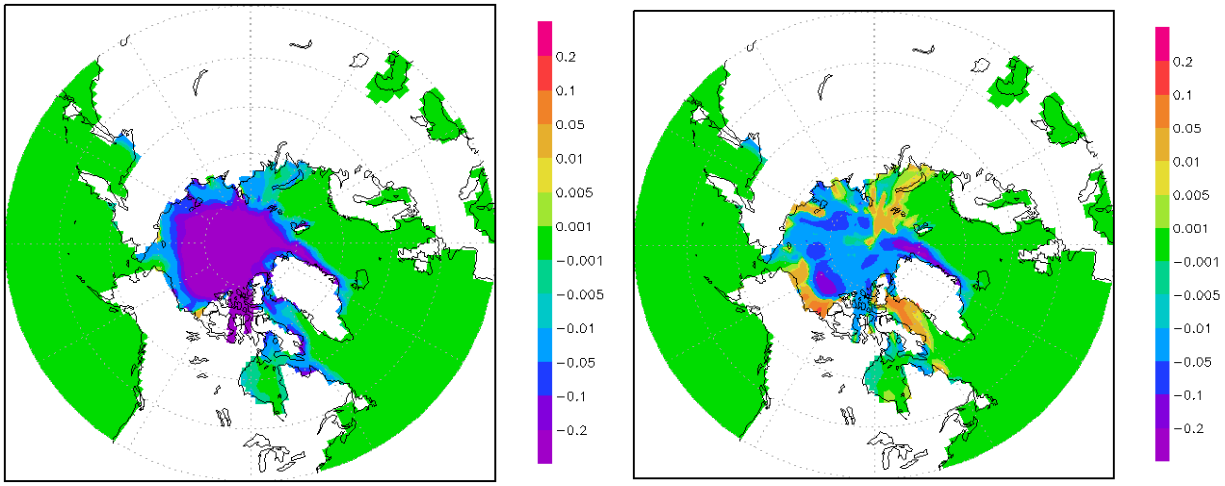

(a) (c)

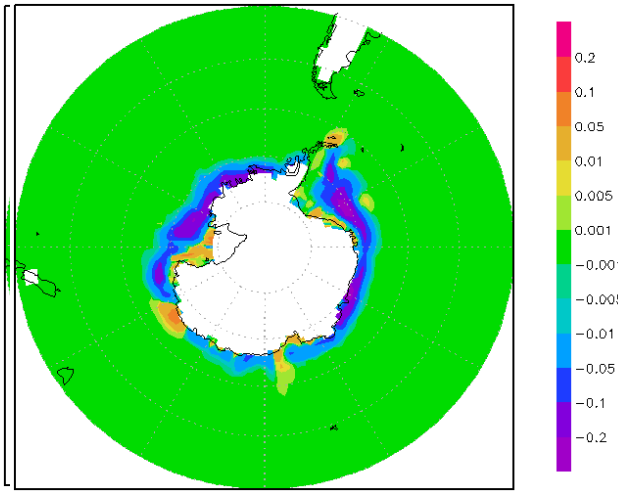

(b) (d)

Figure 3. *Comparison of the North and South polar sea ice fraction averaged over the summer minimum for the final 20 years of the 70 year simulations. Northern minimum is taken as September, and the Southern minimum is taken as March. Panels (a) & (b) show the difference in North and South polar sea ice fraction between Case B and Case A. Panels (c) & (d) show the difference in North and South polar sea ice fraction between Case C and Case A*

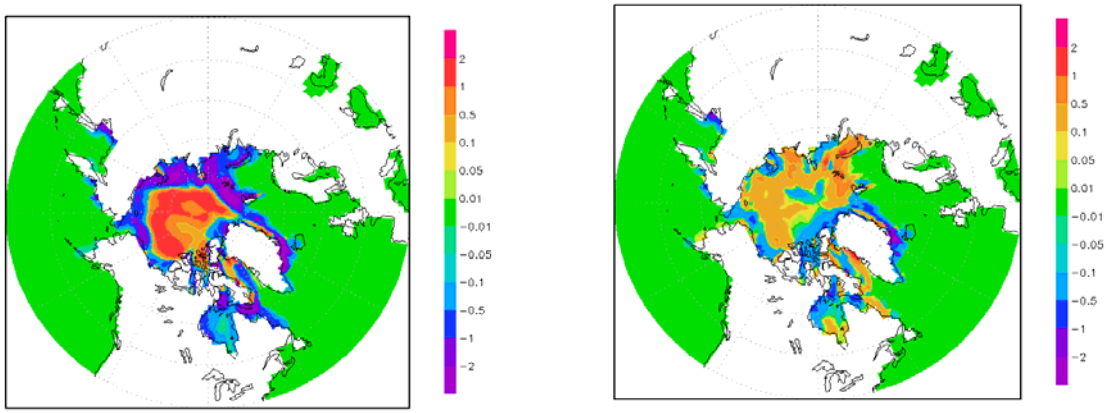

(a) (c)

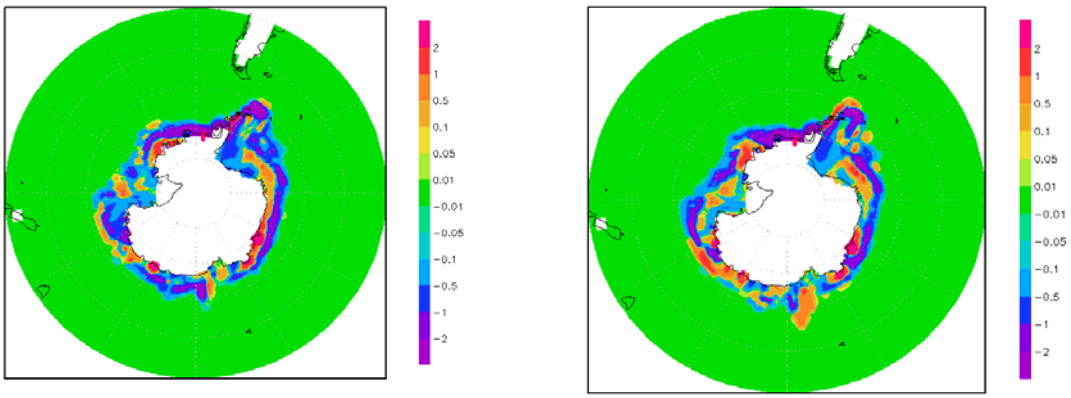

(b) (d)

Figure 4*. Comparison of the North and South polar sea ice thickness averaged over the summer minimum for the final 20 years of 70 year simulations. Northern minimum is taken as September, and the Southern minimum is taken as March. Panels (a) & (b) show the difference in the North and South polar sea ice thickness between Case B and Case A. Panels (c) & (d) show the difference in the North and South polar sea ice thickness between Case C and Case A*

3. Cloud Modelling Relevant to Spray Characteristics and Albedo-Change Values

The purpose of this section is to explore the range of dry salt masses and concentrations that are most effective for altering the albedo of marine boundary layer clouds.

3.1 Explanation of model and set up of runs

We have used a new cloud parcel model with size resolved or bin microphysics that has been developed at Manchester and is called ACPIM (Aerosol-Cloud and Precipitation Interactions Model) (see e.g. Connolly et al, 2009). The work we have carried out here builds on that previously reported in Bower *et al.,* (2006). In their work, the composition of the background aerosol size distributions and that of the added aerosol particles was prescribed to be sodium chloride. The added particles also had a single monomodal size. In this work, the size distributions of the background aerosol distributions are the same as in Bower et al., (2006) but are comprised of ammonium sulphate to which sodium chloride particles are added in a mode of finite width to replicate more realistically the size distributions of particles that can be generated by the spray production techniques described in sections 5.2 and 5.3. The lower limit of added salt particle mass in Bower *et al.*, (2006) was 10**-18 kg, sufficient to cover the range of dry particle sizes under consideration at the time (Salter et al., 2008). However, the range of the mass of added salt particles has now been extended to smaller sizes, to encompass the size-range that can be produced using the Taylor-cone technique (described later), which produces dry salt particles in the mass range ~3.10**20 to 5 x 10**19kg.

The parcel model version of ACPIM used here activates aerosols in a sectional way. ACPIM also uses a more thorough description of the thermodynamics of the aerosol (Topping et al 2005) than

was present in the NEATCHEM model used in the Bower *et al.,* study. Three sets of model runs were performed with ACPIM; in each set of runs the control corresponded to running the model with a `background' aerosol size distribution measured in three different air masses (the clean, medium and dirty distributions used in Bower *et al.,* 2006). Clean corresponds to a total number concentration of ~10 cm^{-3}; medium ~260 cm^{-3} and dirty ~1000 cm^{-3}.

Koehler theory was used to determine the equilibrium vapour pressure of the aerosols (see Topping *et al.*, 2005) in the background size distribution of particles (composed of $(NH_4)_2SO_4$). The initial relative humidity, pressure and temperature in the model were set to 95%, 950 hPa and 283.15 K respectively and the model was run until the parcel was lifted a total of 250m. Typically this generated a cloud base (ie saturation level) ~75m above the starting level and hence a cloud ~175m deep, allowing comparison with the results of Bower *et al.(*2006) Future work will look at the sensitivity of the addition of aerosols to deeper (ie more optically thick) clouds, although (as in the Bower et al. studies) the trends in albedo changes produced are expected to be similar. These simulations were repeated for different prescribed vertical wind-speeds of 0.2ms^{-1}, 0.5ms^{-1} and 1.0ms^{-1} to represent the typical range of updraft speeds found in marine stratocumulus. Sensitivity tests were then performed investigating the effect of adding a log-normal mode of aerosol to the background ammonium sulphate aerosol distributions to simulate the spread in sizes expected from the droplet spray technique. The composition of the particles in the added aerosol mode was NaCl, and their equilibrium vapour pressures were obtained from Koehler theory.

The parameters varied in these tests were the total number of added aerosol particles, n_{add}, and their dry salt mass ms. The parameter values used were n_{add}=0, 30, 300 and 1000 cm^{-3} and ms = 1.x10^{-20}, 3. x10^{-20}, 7. x10^{-20}, 1. x10^{-19}, 3. x10^{-19}, 7. x10^{-19}, 1. x10^{-18}, 1. x10^{-17}, 1. x10^{-16}, 3. x10^{-16}, 1. x10^{-15} kg (or 1.06x10^{-2} , 1.53x10^{-2}, 2.03x10^{-2}, 2.29x10^{-2}, 3.30x10^{-2}, 4.37x10^{-2}, 4.92x10^{-2}, 1.06x10^{-1}, 2.29x10^{-1}, 3.30x10^{-1}, 4.92x10^{-1} μm dry aerosol diameter respectively). The added lognormal mode was specified to have a diameter equal to that of the added dry salt particles, i.e., . ($\bar{d} = \sqrt[3]{6ms/\pi\rho}$). In all cases the standard deviation of the mode was specified to be 0.25. The parameter values listed totalled 41 runs per prescribed updraft value, a grand total of 369 runs (including runs with w=1.0ms^{-1} which lead to smaller particles becoming activated. However, the results are essentially similar to the lower updraft cases so they are not presented here). In principle each of the spray techniques will probably yield its own unique size distribution of NaCl particles, but it is not clear yet what these are. Preliminary results show some sensitivity to the mode width, so it is intended to further investigate this in order to inform spray technology engineers as what tolerance is acceptable vis-à-vis this parameter.

In order to calculate the albedo for the simulation we first calculated the volume extinction coefficient, □(z), by integrating the product of the total cross sectional area of the particles by their scattering efficiency (approximated as 2 in this size regime, which is a valid approximation – see figure 9.21 of Jacobson, 2005):

$$\beta(z) = 2\sum_i N_i \pi d_i^{\,2} / 4$$

where N_i and d_i are the number concentration and diameter of the particles in bin i, and the sum is over every model size bin and each height level in the model. The solar optical depth, □ ???, is then calculated by integrating the volume extinction in the vertical:

$$\tau = \int \beta(z) dz$$

The approximate broad-band albedo, A, is then calculated using the formula (see equation 24.38 of Seinfeld and Pandis, 2006), i.e.

$$A = \frac{\tau}{\tau + 7.7}$$

3.2 Results from model runs

Figure 5 shows results in the case where the background ammonium sulphate size distribution is taken from that measured in a "clean air mass" (Bower *et al.,* 2006). This case represents the most pristine conditions we might expect to find in the maritime boundary layer. Concentrations in the medium case are slightly higher than found over the SEP (eg during the recent VOCALS experiment). The dirty case is very polluted. For the clean case, it can be seen (Figure 5) that adding NaCl particles of dry mass less than approximately 1 $x10^{-19}$ kg results in no change to the cloud drop number since these particles have too high curvature and too low solute mass to be active CCN. Adding particles of dry mass greater than ~1 $x10^{-16}$ kg results in aerosols not activating to form cloud drops (Figure 5(a) and (b)). However, the added sodium chloride aerosols, while not "classically" activating (to form cloud drops), still take on appreciable liquid water, swelling to sizes approaching ~10 μm. The result of this is a thick haze having high extinction of solar radiation and hence a high albedo, as can be seen from Figure 5(c) and (d). The pre-existing ammonium sulphate aerosols have their activation suppressed. Between 1 $x10^{-19}$ and 1 $x10^{-16}$ kg dry mass, we are able to alter the modelled cloud drop concentration very effectively by changing the number concentration of added aerosols. Although the addition of NaCl particles of mass greater than 1 $x10^{-16}$ kg results in no aerosols being activated as CCN, the swelling of these aerosols still has the desired effect of increasing "cloud" albedo, whether they are activated or not. However, adding aerosols of this size or greater (which are effectively giant CCN) may result in undesirable effects such as the more efficient production of warm rain; an effect which will be investigated in future work). The maximum change in albedo for the clean air mass is around 0.4, rising from an albedo of 20% for the control to 60% for the case in which high concentrations of large NaCl particles have been added.

The pattern of aerosols not strictly being activated but still contributing to albedo change was observed in both the medium and dirty cases, so the plots of cloud drop number are not shown here.

Figure 6(a) and (b**)** show the model results for the medium loading ammonium sulphate background air-mass case (Bower *et al.,* 2006). Qualitatively the results are similar to the cleaner air mass results except for two key differences: (i) the magnitude of albedo change is about a factor of 3 smaller than in the clean case and (ii) for the lower updraught case ($w=0.2ms^{-1}$) adding relatively few large NaCl particles may actually reduce the albedo of the clouds by a small amount. The reason for this is that a few large NaCl particles are able to reduce the peak supersaturation in the rising parcel enough to reduce the number of cloud drops in the background spectrum that would otherwise activate to form cloud drops, but not enough to suppress activation entirely. This reduction in turn reduces the extinction of the clouds as there are fewer, larger particles than in the control case. Suppressing activation entirely (i.e. when adding many large NaCl particles) results in many large swollen aerosol particles and hence larger extinction as can be seen from Figures 6(a) and (b). In the absence of seeding, the concentrations of cloud droplets generated in the background clean, medium and dirty cases, were 8.8, 142, 358 cm^{-3} respectively for an updraught of 0.2 ms^{-1}, and 9.8, 180 and 639 cm^{-3} respectively for an updraught of 0.5 ms^{-1}.

Figure 6(c) and (d) show the model results for the case where there is a high concentration of background ammonium sulphate aerosol present, corresponding to a "dirty air mass". Qualitatively the results are much the same as for both the clean and the medium air mass cases. One difference is that the albedo of the clouds is now less susceptible to the inclusion of additional sea salt aerosol. There was little increase in cloud droplet number even when adding particles approaching 1 $x10^{-18}$ kg in mass, especially for the low updraught case (not shown here).

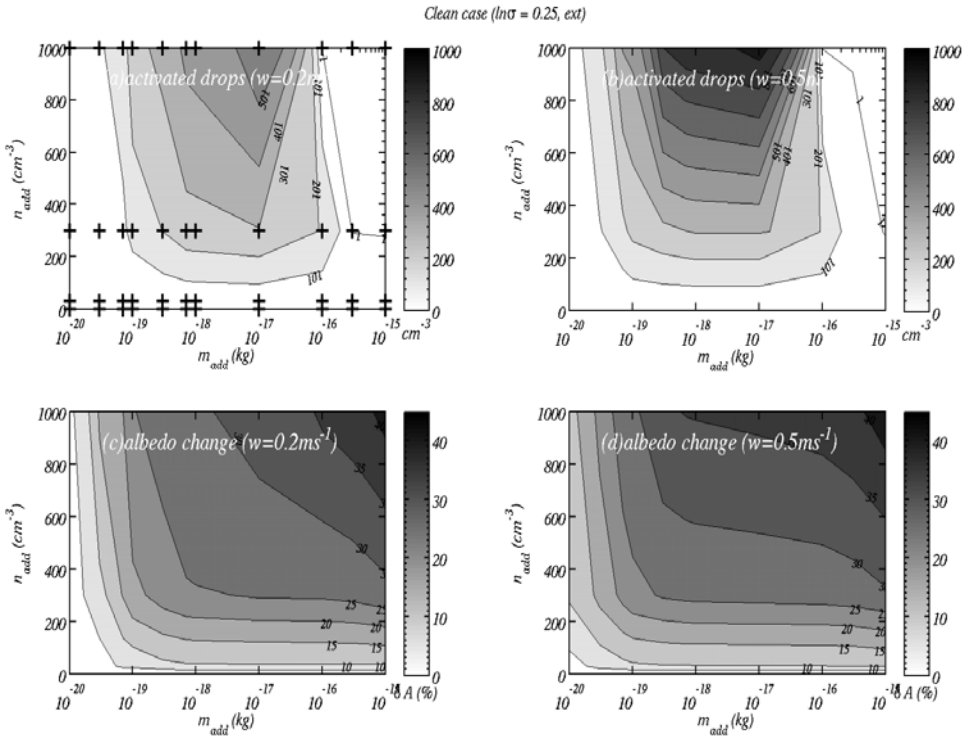

Figure 5. *Summary plots for the clean air mass. The number of activated drops without the addition of NaCl were 8.8 cm^{-3} and 9.8 cm^{-3} for w=0.2ms^{-1} and 0.5ms^{-1} respectively. (a) shows a contour of the number of activated cloud drops when a distribution of NaCl aerosols of different total number and median mass are added to a rising parcel moving at 0.2ms^{-1}. The masses added are on the x-axis, while the corresponding number added is on the y-axis. Plus signs denote the different runs used to calculate the contour plot; (b) same as (a) but for an updraught of 0.5 ms^{-1}; (c) shows the change in the albedo of the clouds resulting from seeding (d) as (c) but for 0.5 ms^{-1}. Please refer to initial conditions in text for dry diameters corresponding to added dry particle masses ms.*

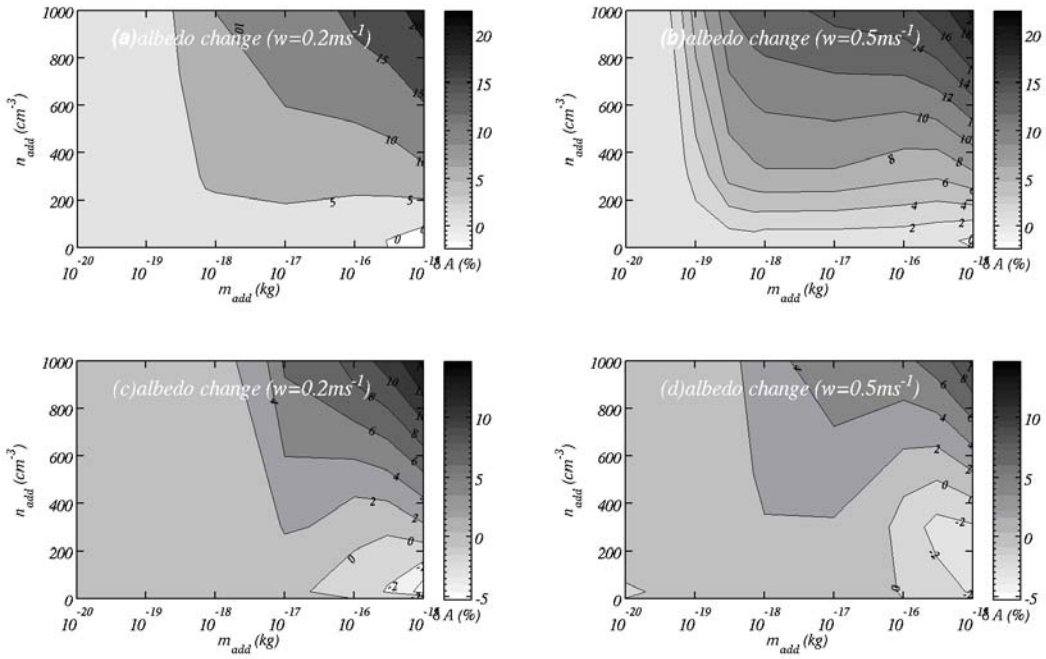

Figure 6. *Summary plots of the albedo change for the medium and dirty air mass cases. For the medium case the number of activated drops without the addition of NaCl were 142 cm^{-3} and 179 cm^{-3} for w=0.2ms^{-1} and 0.5ms^{-1} respectively, while for the dirty case these were 358 cm^{-3} and 639 cm^{-3} for w=0.2ms^{-1} and 0.5ms^{-1}. (a) is the albedo change for the medium case with 0.2ms^{-1} updraught; (b) is the same but for 0.5 ms^{-1}; (c) and (d) are the corresponding contours of albedo change for the dirty case.*

In the medium and clean cases a larger increase in cloud droplet number was found for the addition of NaCl aerosol of this or even smaller mass. The reason for this decreased sensitivity is that in the dirty case there are already copious $(NH_4)_2SO_4$ particles present in the background aerosol to deplete the supersaturation at cloud base such that the NaCl particles of ~1 x10^{-18} kg cannot be activated. Similarly, the point at which drops cease to be activated has also changed. In the previous cases drops ceased to activate when NaCl particles of mass ~1 x10^{-16} kg (or larger) were added. In this case, activation of additional drops ceases at a lower threshold sea salt particle mass (typically 7 x10^{-17} kg or less). This is because the higher concentration of background aerosol contributes significantly to the reduction in supersaturation in the rising parcel of air, suppressing further activation. Another notable difference is that the maximum change in albedo that is achieved is considerably less than for the clean case, and slightly less than in the medium case too. More noticeable in this case is a region where a reduction in albedo occurs when adding relatively few large-mass NaCl particles.

3.3 Conclusions:

The modelling suggests the following:

- The enhancement to the albedo is greatest for clean background conditions. This is consistent with previous work (Bower et al., 2006).
- In the clean conditions the albedo of the control case cloud was approximately 20% whereas for the case where many large NaCl particles were added it was ~60%. This (factor of three) difference should be easily observable in a field campaign. In the medium and dirty cases these increases in albedo were a factor of 1.6 and 1.3 respectively. The

magnitude of these changes will vary slightly with cloud depth (although the trends will be similar), and this will be investigated in future work

- For both the medium and dirty cases a reduction in cloud albedo was found when adding relatively low concentrations of particles that have NaCl masses of ~1 $x10^{-16}$ and greater. This underscores our original proposal that for efficient albedo-enhancement the added particles should have masses higher than almost all natural particles and be in significantly higher numbers. Furthermore, adding particles of salt-mass less than 1 $x10^{-19}$ kg in the clean and medium cases and less than 1 $x10^{-18}$ in the dirty case produced little change to the drop number.
- Adding large NaCl particles may also initiate warm rain (which is undesirable from the geoengineering perspective). This effect needs further investigation both with high resolution models and further parcel modelling

4.. High-Resolution Cloud Modelling

Despite considerable improvements over the last decade (especially in forecast models, e.g. Abel et al. 2010), marine boundary layer (MBL) clouds remain poorly represented in global models (e.g. Wyant et al., 2010) and as such are a critical bottleneck in improved estimation of climate sensitivity in global models (Bony and Dufresne, 2005). The difficulty representing MBL clouds in global models is that many of the processes that control these clouds (e.g. turbulence, entrainment, heat and moisture transports, and precipitation) are not explicitly resolved due to poor model resolutions, and instead need to be parameterized.

Additional aerosols injected into MBL modify clouds through aerosol indirect effects that lie at the heart of the cloud brightening scheme. The first indirect effect, the increase in cloud top reflectivity to incoming solar radiation, was first proposed by Twomey (1974, 1977). It describes how the cloud albedo increases due to an increase in aerosol number in the absence of any macroscale changes in clouds (i.e. changes in cloud cover, thickness, liquid water content etc.). However, it is now known that a number of changes in the macrophysical properties can occur as a result of changes in cloud microphysical properties. Reduction in droplet size as a result of increasing droplet number may suppress precipitation (Albrecht, 1989), which may lead to a further enhancement of cloud albedo by increasing boundary layer moisture or reduction of cloud albedo through increasing entrainment of dry free-tropospheric air (e.g. Ackerman et al. 2004; Wood 2007; Ackerman et al. 2009). Recent in-situ and satellite remote sensing observations are indicating precipitation in MBL clouds seems to be the rule rather than the exception (Leon et al. 2008, Kubar et al. 2009, Bretherton et al. 2010). Change in precipitation induced by aerosols can drive mesoscale circulations that determine cloud structures (Wang and Feingold 2009a, b; Feingold et al. 2010). When considering the deployment of cloud brightening over large tracts of the world's oceans, it will therefore be essential to better understand how precipitating clouds respond to increases in CCN.

Other secondary effects may occur as a result of cloud microphysical changes such as changes to the evaporation and condensation rates in cloud (e.g. Wang et al. 2003) and changes in entrainment driven by reduced sedimentation rates of cloud droplets near cloud top (Bretherton et al. 2007). The ultimate cloud albedo response is a result of numerous complex processes interacting (see e.g. review by Stevens and Feingold 2009). All these associated effects and processes make the parameterization of MBL clouds in global models a real challenge.

High-resolution numerical cloud modelling provides a useful tool that can help improve process-level understanding and provides a necessary and critical test of the efficiency of cloud brightening. To date, only a very few cloud resolving simulations have explicitly attempted to simulate the effects of seeding marine low clouds from a point source. Using cloud-system resolving model simulations, Wang and Feingold (2009a) demonstrated that the concentration of CCN in the boundary layer can help determine whether marine stratocumulus clouds adopt open or closed cellular structures, with significant implications for overall albedo. More relevant to cloud brightening, however, is that once the cloud cellular structures are established, they tend to resist

change and don't necessarily follow conventional aerosol indirect effect responses (Wang and Feingold 2009b; Feingold et al. 2010).

Figure 7 shows the impact of ship emissions on clouds in both clean/precipitating and polluted/non-precipitating environments. An open-cell structure forms in the precipitating case. A ship track is clearly visible in the cloud albedo field (Figure. 7a) for the clean/precipitating case as would be expected even with Twomey's argument. However, there are subtle changes in the cellular structure along the track from the plume head to tail, indicating that the interactions among ship-emitted CCN, clouds and precipitation vary with time. As revealed by Wang and Feingold (2009b), precipitation is suppressed most in the central section of the track, while new and sometimes stronger precipitation develops some distance behind the plume head, resulting in restoration of the open-cell structure. This, together with the less reflective dark regions close to the lateral boundaries of the ship track, is caused by a mesoscale circulation owing to dynamical feedbacks associated with the initial suppression of precipitation along the ship track. Convergent branches of the local circulation, located in the lower boundary layer over the track, pump moisture from the regions adjacent to the track, and divergence in clouds helps dilute the ship-emitted CCN. Quantitatively, cloud albedo along the ship track was enhanced by 0.08 (averaged over 10 hours; Wang and Feingold 2009b), while the domain average albedo was only 0.015 higher than that of un-seeded clouds. The dark edges (Figure 7a) partly cancelled out albedo enhancement along the ship track.

Although ship emissions are the same in the polluted/non-precipitating case, the ship track in Figure 7b is nearly invisible because the relatively small enhancement in cloud albedo (an average of 0.02; 4.3% relative to the domain average) is masked by the highly reflective cloud background. In addition, there is no dynamical feedback associated with the interaction between the CCN perturbation and precipitation since the polluted cloud is non-precipitating. When averaged over the entire domain, the albedo enhancement in the polluted case becomes even smaller, 0.005.

Formed in a sufficiently polluted environment, closed cells as shown in Figure 7b are over two times brighter than open cells in Figure 7a. The most ideal outcome of cloud seeding/brightening would be turning open cells into closed ones as suggested by Rosenfeld et al. (2006). Can an influx of aerosols close open cells? There is no clear and firm answer yet. Numerical experiments conducted by Wang and Feingold (2009b) suggest that once the open-cell structure has formed, simply adding more aerosol particles, even in large quantities, does not necessarily transform it to closed cellular structure.

These high-resolution modelling studies suggest that seeding marine stratocumulus clouds, especially those that are precipitating, is more complicated than conventional aerosol indirect effects predict. The albedo response depends on meteorological conditions, background aerosol concentrations and seeding strategy, which together determine whether or not the clouds precipitate and therefore whether or precipitation-suppression feedbacks can operate. Wang et al. (2010; manuscript in preparation) describe more details of different meteorological and microphysical scenarios in this context, providing implications for experimental strategies to adopt in the field.

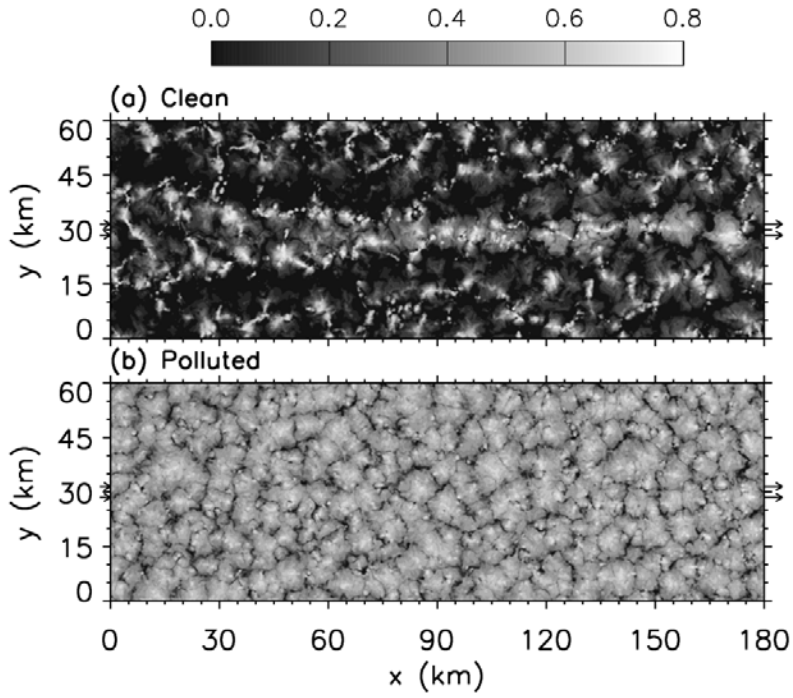

Figure 7*: Snapshots of cloud albedo field when ships pass through the domain once from x = 0 to 180 km, about 7 hours after the start of the simulations. The background aerosol number concentration varies linearly from a lower bound at x = 0 to an upper bound at x = 180 km; (a) clean case 60 – 150 mg^{-1}, and the (b) polluted case 210 – 300 mg^{-1}. Arrows indicate the direction of movement of the ships and the band of ship plumes emitted near the surface. Details on the model and experimental setup can be found in Wang and Feingold (2009a, b).*

The inability of global models to adequately represent MBL clouds and the unresolved complexities of aerosol-cloud-precipitation interactions in such clouds are major limitations in the assessment of the Earth System response to future changes in climate, regardless of whether the change was caused inadvertently or was deliberately engineered. Improving our knowledge of such processes should therefore be a major research goal, which relies much on high-resolution modelling. We suggest that any future research program on cloud brightening should include a high-resolution cloud modelling component. More work is necessary to understand how ship-tracks such as those shown above form in response to idealized seeding strategies under different meteorological conditions and with different aerosol background states (e.g. Wang et al. 2010). Beyond this, high resolution modelling should be used to assess the interaction of plumes from multiple seeding platforms such as those that would be necessary to deploy cloud brightening as a geoengineering scheme regionally or globally. We currently have little idea how clouds would respond to multiple aerosol plumes, and yet Figure 7a and Wang et al. (2010) suggest that there are regions where the induced mesoscale flows in the boundary layer act constructively and other regions where they destroy clouds, producing unintended consequences that reduce expected albedo response. High-resolution cloud modelling can also be used to examine how rapidly induced aerosol perturbations from seeding are removed by coalescence scavenging and dilution from entrainment of free-tropospheric air. These issues will be particularly pertinent when designing field experiments to test critical aspects of cloud brightening.

5. Technological Work on Marine Cloud Brightening

5.1 Introduction

In this section we describe technological work performed to date on the marine cloud brightening geoengineering idea. First, we provide information on two separate seawater spray production techniques that we are examining: via microfabrication lithography and electrohydrodynamic instability. We then outline results from the model described in Section 3, designed to determine the conditions under which the latter spraying technique could produce significant albedo enhancement. Finally, we present some computational fluid mechanical studies of the stability of Flettner-rotor wind-powered vessels, which might be used for spray dissemination (Salter et al. 2008).

5.2 Spray Production via Microfabrication Lithography

This technique for producing seawater spray droplets is described in detail by Salter et al. (2008), so will simply be outlined herein.

It is proposed that each of the Flettner Rotor spray vessels be fitted with about 28 billion nozzles of chosen diameter in the region of 1um, produced by a method based on micro-fabrication lithography. Droplets are formed by forcing filtered seawater through the nozzles etched in 200 mm diameter silicon wafers. Spraying the required 30 litres per second through a pressure difference of 10 bar needs a power of only 30 kilowatts. Controlled piezo-electric excitation allows the drop-size to be varied over a significant range.

Natural sea-water contains large amounts of material which can clog micrometre diameter nozzles but the requirements for reverse osmosis are far more stringent: the feed to reverse osmosis plant is taken from water much closer to land.

Fortunately the technology for ultra-filtration is now well developed and volumes being filtered are already larger than will be needed for the cancellation of a doubling of pre-industrial CO2. Before the introduction of the Salk vaccine, filters were developed to remove 30 nm polio viruses from drinking water. The key requirement is frequent back flushing. The design uses a set of eight Norit X-flow Seaguard filters for each rotor of the spray vessel. One of the eight is always being back-flushed with one seventh of the output of the others.

This spray-system could also be mounted on more conventional vessels. It is hoped to test it in the near future.

5.3 Electrohydrodynamic Spray Fabrication

We have explored experimentally a number of ways to produce seawater droplets that would be suitable for use in cloud brightening. The critical requirement is that their salt-mass ms be high enough that it can convert into cloud droplets at supersaturations S occurring in marine stratocumulus clouds. S depends on updraught speed, and the properties of the air-mass. Cloud modelling described below provides values of critical mass for a variety of relevant scenarios. They show that significant droplet formation and associated cloud albedo increase can occur for ms values down to about 5×10^{-20} kg. Hence the initially sprayed droplets should be not less than about 150–200 nm in diameter. For energy efficiency, it is advantageous to make the droplets as close as possible to this lower acceptable limit. It is the number of suitable nuclei formed, not the amount of water sprayed that is important. Also, the smaller the salt-mass and size of the droplets capable of inducing activation, the smaller the negative buoyancy created by the evaporation of spray particles, which could possibly inhibit their ascent.

We investigated the performance of standard commercial nozzles that are used in fogging systems, toroidal vortex-based nozzles, colliding water jets, ultrahigh pressure nozzles (420 MPa), and Rayleigh-mode jet breakup from micromachined and radiation-track apertures. These

experiments will be detailed in another publication, but so far none has produced encouraging results.

The most promising results so far were obtained using Taylor cone-jets, drawn from porous tips. The phenomenon of electrospray, first observed by Zeleny (1917) and examined in detail by Taylor (1964) is now extensively used in mass-spectroscopy, and arrays of Taylor cone-jet capillaries are used as micro-thrusters for satellites. Upon application of a voltage to a capillary containing a fluid, the most interesting of the spraying modes is the cone-jet, i.e., a cone terminating in an emerging jet. The 49.3° half-angle cone first described by Taylor occurs when the electric field and the surface tension are in quasi-equilibrium. The radius of the cone allows the determination of the electric field at the surface. The jet description is much more complex, particularly for high-conductivity liquids such as seawater. Analyses by De la Mora (2007) and Gañán-Calvo *et al*. (2009) show that a critical radius (r_i) exists, defined such that the volume of the cone from this radius to the apex, divided by the imposed flow-rate, is equal to the dielectric relaxation time of the fluid. The highly charged jet of approximate radius 0.2 r_i that emanates, breaks up in a tight fashion similar to that of an uncharged Rayleigh jet. Each drop is often accompanied by a satellite drop of mass a few percent of that of its parent.

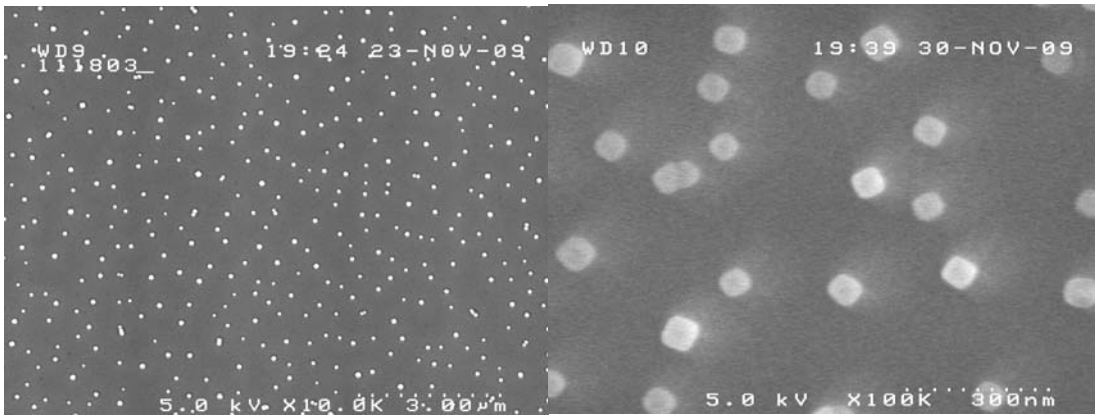

Figure 8 SEM images of salt particles from 3.5 wt% saltwater cone-jets at different magnifications.

Figure 8 shows SEM images, at different magnifications, of salt particles produced by a Taylor cone emanating from a porous tip, collected on a silicon wafer at a 5.4 kV potential, a current of 0.2 µA with a flow of 5.6 nL s^{-1}, using 540 ppm of surfactant. The surfactant was found to eliminate the corona discharge that destroys the uniformity of the particle distribution. The average size of these crystals is on the order of 75–85 nm, almost ideal for the intended purpose. The droplets evaporate before they reach the silicon wafer 2 cm away. This almost instantaneous evaporation of the droplets is due to their emergence from the jet with velocities approaching the speed of sound, and the heating that takes place in the cone itself (Crowley 1977). Boiling bubble formation is observed under high current conditions. These particles readily activated at a supersaturation of 0.5%, achieved by cooling the wafer with a thermoelectric chuck in an enclosed environment.

Although each cone jet produces a large number of droplets (on the order of 10^8–10^9 sec^{-1}), scale-up requires 10^8 jets to reach roughly 10^{17} CCN s^{-1} per sprayer, as required at the CO2-doubling point (Salter et al., 2010). Small arrays of porous tips work well, but the overall size would be prohibitive. Various efforts have been made to mass-produce cone jet capillaries and associated extraction plates. Perhaps the most relevant work is by Deng *et al.* (2009), who describe the micro-machining of silicon capillaries and extraction plates, alignment methods and the production of arrays with up to 331 nozzles, producing remarkably uniform spray, with only a few percent of size deviation. The density of the capillaries exceeds 100 mm^{-2}, suggesting approximately 1 m^2 in total for the nozzle array.

As a low cost alternative, we have pursued the use of holes in low dielectric polymeric materials (PEEK, polyimide, PMP) in place of capillaries. This approach was first outlined by Lozano *et al*. (2004), and Bocanegra *et al*. (2005). This technique would lower power consumption, and the fabrication of holes is significantly easier than that of capillaries. These holes must have a high aspect ratio in order to avoid interaction between adjacent holes. This can be overcome by using a dielectric film thick enough (50–75 μm) to provide the electrostatic field enhancement, attached to a porous block that provides flow impedance isolation and filtration at the same time. Such arrays may then be made by fast and inexpensive laser drilling systems. To fabricate prototypes we were able to make use of a Samurai UV marking system (courtesy of DPSS Lasers), capable of drilling 50,000 holes s^{-1}. Hence the drilling of 100 million holes is a manageable task, requiring a 20–30-μm hole every 100 μm over 1 m².

The other requirement (Lozano *et* al. 2004) is that the water needs to be confined at the rim of each individual hole, or jets will coalesce. To this end, it has been found that the dielectric material needs to be made superhydrophobic, i.e., the fluid contact angle must be in excess of 150° (Byun *et al*. 2008). Polyimide films were readily made superhydrophobic by plasma etching with oxygen, yielding a rough surface, followed by plasma deposition of a 20-nm fluorocarbon film. The combination gives rise to the desired surface properties, with water contact angles approaching 160°. However, the surfactant needed to obtain reliable cone-jet spraying of seawater lowers the contact angle to values that are unacceptable. Using films made at the Stanford Nanofabrication Facility or supplied by commercial sources (Repellix™) we have been unable to find a combination of surfactant and robust surface preparation that satisfies all the requirements.

The surfactant requirement can be eliminated if the ambient pressure is raised slightly (20%). The air breakdown field increases with decreasing jet radius because of the very limited extent over which electron multiplication can take place when the spatial field is itself restricted. The field can also be enhanced by increasing the ambient air pressure, which decreases the electron mean free path and again limits the probability of avalanche occurrence. Hence with slight pressurization, corona disappears and there is no need for surfactants. Raising the pressure causes airflow through the extraction apertures, and while the flow through each hole is small, an array of 100 million holes necessitates using about 270 kW of pneumatic power The flow of air is of course beneficial in helping the passage of the droplets through the extractor holes. When the capillary holes are smaller than 10 μm, the air breakdown field is at all times higher than the field over the cone itself, so neither surfactant nor pressurization is needed.

In summary, the fabrication of large arrays of Taylor cones, either by silicon micro-machining or by laser drilling in dielectric sheets, seems quite feasible although no such large arrays have yet been constructed. It is estimated, that for an array of 100 million holes, roughly 1 m² in size, the electrical power requirement would be less than 100 kW. If airflow is used there would be an additional requirement of 270 kW for pneumatic power. Since over 90% of the electrical power ends up as droplet kinetic energy, it can probably be recovered by reverse induction using a Kelvin arrangement.

As a simpler alternative, we are exploring the spraying of seawater at or near its critical point. In this regime, water has little or no surface tension and a gas-like viscosity and hence should produce fine dispersions. This has been demonstrated in the pharmaceutical industry with the spraying of supercritical CO_2 containing dissolved therapeutic compounds. While the distributions resulting from this technique are bound to be wider than those from cone-jets, the resultant particle distribution can on occasion be quite uniform (Reverchon & Spada 2004). Results of this investigation will be reported later.

We used the model described in Section 3 to examine in more detail the conditions under which the electrohydrodynamic spraying technique could produce albedo–change values of significance (i.e. not less than about 0.06, or 6%). We have tabulated, in Table 1, the change in albedo (for each air-mass) that could be achieved by adding 1000 cm^{-3} of NaCl particles of mass within the range currently achievable by this technique (i.e. up to about 10^{-19} kg). We see that the technique

can result in large albedo-change in clean air masses. For the medium polluted air mass only particles of salt mass larger than about ~$3x10^{-19}$ kg result in a albedo-change that may be significant for offsetting warming by CO_2, whereas for the dirty airmass all salt masses result in a negligible albedo-change.

This highlights that in very clean clouds the electrohydrodynamic spray technique is feasible. However, in the medium and in particular the dirty air masses we would probably need to produce larger particles of (around $1x10^{-18}$ kg) as suggested by Figure 6.

Table 1: ΔA values (in percent) achieved in the 0.2ms^{-1} updraught case for runs where 1000cm^{-3} of NaCl were added in the range 1x10^{-20} to 3x10^{-19} kg.

Airmass	**Mass (kg) 1x10^{-20}**	**3x10^{-20}**	**7x10^{-20}**	**1x10^{-19}**	**3x10^{-19}**
Clean	3.9	16	20	25	28
Medium	$9.1x10^{-3}$	$3.8x10^{-2}$	$5x10^{-1}$	1.4	6.5
Dirty	$1x10^{-2}$	$2.3x10^{-2}$	$4.7x10^{-2}$	$6.5x10^{-2}$	$1.8x10^{-1}$

5.4 CFD Studies for Optimizing a Low-Carbon, Sea-Going Propulsive System

Scene Setting

The previous section has outlined possible design routes for an atomizer that will create a stream of microscopic salt-water droplets to act as the source of additional CCN. The major remaining engineering-design task is that of providing a vessel – or, rather, fleet of vessels – that will distribute the sprays where their effect will be most productive. Salter et al. (2008) have argued that propulsion of these craft by Flettner rotors is the optimum way to proceed. A Flettner rotor (named after its inventor, Anton Flettner) is a vertically mounted cylinder that may be rotated about its axis by an external power supply. When air flows past it, the cylinder rotation creates a force (the Magnus force) at right angles to the air flow that propels the vessel on which the cylinder is mounted. The rotor thus plays the same role as the sails on a yacht but the thrust levels attainable are far greater than for a sail of the same area and, moreover, the control of such vessels is very much simpler (without the complex rigging of a sail and with far superior manœuvrability) making them ideal for un-manned, radio-controlled operation. Moreover, it has been estimated, Salter et al. (2008), that the cost of providing the power to spin the rotor is an order of magnitude less than that required for a screw-driven vessel of comparable size sailing at the same speed.

An artist's impression of such a vessel is shown in Figure 9. While the original Flettner vessel which crossed the Atlantic in 1926 was propelled by two purely cylindrical rotors, in the conceptual design of the cloud-seeding craft shown in the figure, the rotors have a number of discs mounted along their length. The inclusion of such discs had been shown by Thom (1934) to improve rotor performance at high spin rates. Inevitably, however, the scope of that experimental exploration was limited and was certainly not conceived as contributing to the particular requirements of the cloud-seeding craft. Moreover, nearly 80 years on, as in so many areas, computer simulation (while not replacing the need for experiments) has made it feasible to explore a wide range of flow conditions and rotor geometries relatively rapidly and to provide far greater detail than any experiment. Here the first results of applying *computational fluid dynamics* (CFD) to the Flettner rotor problem are presented.

The first major computational study into the behaviour of flow past a rotating cylinder was undertaken by Mittal & Kumar (2003) (hereafter M&K). While their study was limited to laminar flows at Reynolds numbers two or three orders of magnitude below those that would be encountered in an actual cloud-seeding vessel, their results revealed a potentially worrying feature with a major bearing on the present research. Over a limited range of rotation rates (relative to the wind speed) the flow around the cylinder experienced large-scale temporal periodicities that produced highly undesirable variations in drag and lateral forces on the cylinder. If these were present under

operational conditions in the cloud-seeding vessel they would, *inter alia*, have a seriously adverse effect on the lifetime of the rotor and its support mechanisms. Thus, in the exploratory studies presented below of turbulent flow past the rotor at Reynolds numbers typical of operating conditions, such flow instabilities have been a major feature to watch out for.

Numerical and Physical Model

Computations have been performed using an in-house CFD solver, STREAM (Lien & Leschziner, 1994), to examine the flow around rotating cylinders with and without Thom discs. For these tests the discs have been taken as flat annular plates of diameter twice that of the cylinder, axially spaced, one cylinder diameter apart. (In Thom's original tests the disc diameter was three times that of the rotor and the axial spacing just half the rotor diameter.) The results presented here have been obtained using a multi-block, non-orthogonal grid of around 0.75M cells, covering a domain extending far enough from the cylinder for boundary effects to be negligible, and extending vertically from one disc to the next, as shown in Figure 8. A uniform "wind" velocity was specified around the inlet part of the outer boundary and zero-gradient conditions on the outlet. Symmetry conditions were applied along the two boundaries normal to the cylinder, and no-slip conditions, via "wall functions", were applied at the disc and cylinder surfaces. For comparison, simulations were also performed for a bare cylinder (i.e. without discs).

For most of the test cases the effects of turbulence were represented by a conventional *k-ε* linear eddy-viscosity model with standard log-law-based wall functions to provide the wall boundary condition. Some runs have, however, been made using more advanced stress-transport turbulence models and wall-function treatments (summarized, for example, in Craft et al, 2004). Although there are some quantitative differences in results between the different modelling approaches, cross-checks show very similar trends.

Initial Computational Results

To validate the procedure, purely laminar flow around a bare rotor for a Reynolds number of 200 was examined, corresponding to the case studied by M&K. In agreement with their results, the present computations confirmed that the Karman vortex street, present behind a non-rotating cylinder, disappeared for dimensionless rotation rates, $\Omega \equiv \omega D/\left(2W_\infty\right)$, greater than 2 (where ω and *D* are the angular velocity and diameter of the cylinder and W_∞ is the 'wind' speed). For a narrow band of rotation rates around Ω=4.4, longer-period, large-amplitude oscillations developed, although by Ω=5 these also disappeared, again broadly in agreement with the M&K results. As noted above, a major question in the present context is whether these instabilities also arise in turbulent flow at the much higher Reynolds numbers commonly encountered for a Flettner rotor.

The presently-predicted results for turbulent flow at Re = $8\text{x}10^5$ appear in Figure C in the form of time histories of the lift coefficient, C_L, at a number of non-dimensional rotation rates. For zero rotation the bare cylinder results display the expected oscillatory pattern associated with the Karman vortex street. As the rotation in increased these oscillations disappear, and the magnitude of C_L increases steadily. By a rotation rate of Ω=5 a lift coefficient of around 12 is predicted. Although rather less than half the corresponding value found for laminar flow, this is still sufficiently high to underline the value of the Flettner rotor as a propulsive device. A further point to note from the bare cylinder results is that the large-amplitude oscillations seen in the laminar flow calculations around Ω=4.4 were not detected in the turbulent case for the rotation rates examined. However, as can be seen from Figure 9, at rotation rates above Ω=3 the solution did not exhibit an entirely steady behaviour, indicating that there are nevertheless unsteady 3-dimensional structures present in the flow, albeit not in an organized, regularly repeating form.

Turning now to the effects of the Thom discs, the time histories of the lift coefficient, also included in Figure 11, indicate that the mean values of C_L are not very different from those of the bare cylinder. A feature worth noting, however, is that, by including the discs. a much steadier flow field is achieved. For the case of no rotation, the Karman vortex street is suppressed, and a constant value of C_L (zero) is

thus returned. At rotation rates of Ω=3 and 5, although there are some small undulations in the C_L time history, these are very minor (and fairly periodic) compared to the behaviour of the bare cylinder.

Figure 12 compares the predicted mean lift coefficient, as a function of rotation rate, with and without discs and the very early (but still the most comprehensive) measurements of Reid (1924) for a bare cylinder. The experimental data for the bare cylinder show a fairly rapid rise in C_L as Ω is increased from zero to around 3, followed by a more moderate rate of increase thereafter. The present results broadly reproduce this pattern. The numerical results show values slightly higher than the measurements. As noted earlier, the calculations show only minor differences in average C_L values between the cases with and without Thom discs.

Finally, the question of whether or not large-amplitude periodicities may arise cannot yet be answered definitively. The computations of M&K and our own show that in the laminar-flow regime these instabilities appeared only over a very narrow range of spin rates. Preliminary turbulent flow studies have suggested that such oscillations may also occur, e.g. Craft et al. (2010), again over a narrow range of conditions. Further extensive explorations are required, however, before authoritative conclusions can be reached.

***Figure 9**. Artist's impression of a Flettner rotor ship ©J. MacNeill (2008)*

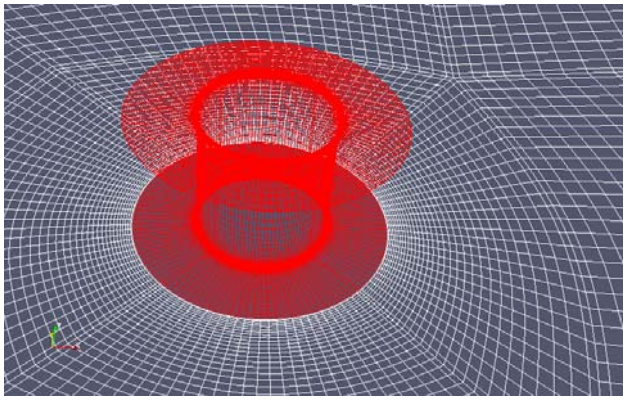

Figure 10. *Details of the multi-block, non-orthogonal mesh.*

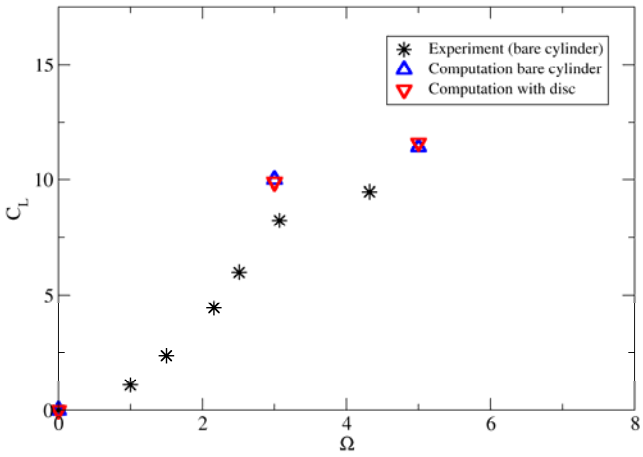

Figure 11*. Predicted temporal evolution of lift coefficient for turbulent flow at Re=8x10^5, for a range of rotation rates.*

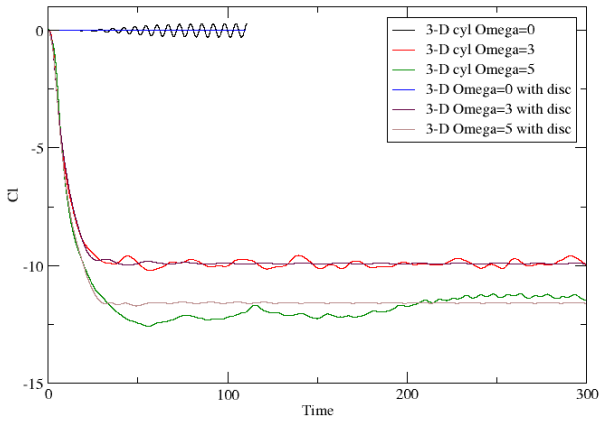

Figure 12. *Mean lift coefficients for bare cylinder and cylinder with discs over a range of rotation numbers. Experimental measurements for bare cylinder, from Reid (1924).*

Examples of Future Work

Readers will recognize that the results above, while containing interesting and encouraging pointers, represent just a start on a range of CFD comparisons that will need to be made. As a first step the computations need to consider a complete rotor rather than just the section between one disc and the next. This will enable the exploration of end effects and the possible variation with height of the wind velocity to be examined as well as potential interference effects between the rotors (if, as in Figure 9**,** a multi-rotor vessel is chosen). The effect of heeling of the ship (even by only around 2-3°) on the rotor's aerodynamic performance also needs to be examined. As a final example of issues requiring examination, we note the possible effects of the top disc of the rotor on the behaviour of the salt-water spray discharge. One may well wish to cause the spray to spread as quickly as possible to minimize the risk of droplet collisions (which would create larger than optimal size of droplets). It is known that imparting swirl to the spray will do that. However, that will lead to a reduction in the droplets' vertical velocity which, on its own, may reduce the proportion of salt particles reaching the cloud base. Such competing effects and their consequences need to be considered in the next phases of this research

6.. A limited area experiment to explore the fundamental processes involved in marine cloud brightening

Before any geoengineering scheme based on solar radiation management could be implemented it first must fulfill the following criteria a) it can deliver the desired agent by which solar radiation will be scattered to space (sulfate particles in the case of a stratospheric aerosol and increases in sea spray aerosol in the case of cloud brightening) ; b) it can deliver the desired radiative response; and c) the climate responses to such perturbations are small compared to those associated with changes induced in the climate system from inadvertent human activity. The last of these cannot be tested by experiment for any of the SRM methods without full implementation lasting multiple years and carries a risk of substantial negative impacts. This was argued by Robock et al. 2010, who focused upon geoengineering through stratospheric sulfur injection, currently considered to be one of the most feasible schemes (Crutzen 2006). Robock et al further argued that it is impossible to field-test any elements of geoengineering technology without significant modification to the climate system. That is, it is not possible to separate field study from actual deployment of geoengineering. For schemes involving stratospheric sulfur injection, this is indeed the case. The climatic response of the scheme is fundamentally derived from the slow spreading of particles in the stratosphere over a significant fraction of the globe. That is, the climate response of injection at a given location is highly non-localized. Furthermore, many thousands of injections of the particle precursor gas sulfur dioxide are necessary to produce a climate response that could significantly cancel those from anthropogenic greenhouse gases, and maintain it in the presence of pre-existing particles. Hence both the sustenance of the technique and its response is inherently global. As such, Robock et al. (2010) are entirely correct in arguing that it would be extremely difficult to measure either an effect on the Earth's radiation budget or maintenance of the aerosol from only a small number of injections that might constitute a field test. Both from the standpoint of maintenance of the sulfate aerosol and the criterion of needing to measure a radiative response, we agree with the notion that *stratospheric sulfur injection* geoengineering cannot be reasonably field tested.

The argument of non-testability cannot be equally applied, however, to all geoengineering schemes. Since aerosol particles in the marine boundary layer are extremely short lived (typically a few days) compared with their stratospheric counterparts (1-2 years), perturbations to the radiative budget from marine cloud brightening are inherently localized. Geoengineering by marine cloud brightening can therefore be construed as an upscaling of many localized perturbations to the Earth's radiative budget. Thus, both the aerosol injections and the radiative responses associated with marine cloud brightening occur over relatively small spatial scales. We argue that this key distinction makes field testing of both the generation of changes in particle properties (criterion a) and the effects on cloud and radiation (criterion b) from the implementation of a cloud brightening spray system possible, in contradiction of Robock's argument.

The stratospheric sulfur injection scheme has to date been considered one of the most viable schemes not least because previous volcanic eruptions such as Pinatubo in 1991 have provided significant data against which model predictions of the radiative effects of sulfate particles in the stratosphere can be tested and validated (Minnis et al., 1993; McCormick et al., 1995). Unlike stratospheric aerosols, many of the basic processes linking aerosols, clouds, precipitation, and radiation underpinning the cloud brightening scheme are rather poorly understood (Stevens and Feingold, 2009). Given that the influence of human activity on such processes has been proposed to make a substantial contribution to the radiative balance (IPCC, 2007 and refs therein), it is imperative that knowledge of the basic interactions is improved substantially regardless of the viability of cloud brightening as a geoengineering scheme.

Inadvertent human induced changes to regional aerosol particle burden have been used to investigate these processes in regions of stratocumulus in the past (e.g. Johnson et al., 2000; Stevens et al., 2003), though large natural variability and co-dependency of processes has to date limited progress towards full understanding. Also, emissions from the stacks of ships have been used to study aerosol-cloud interactions (e.g. Russell et al., 1999) but single plumes of this type can provide only limited information as plumes are narrow and entrainment and mixing are often dominant. A limited area field experiment which provides a substantial and detectable perturbation above the background on spatial scales that are detectable from space could therefore offer a unique way to probe aerosol-cloud-precipitation interactions and their influence on radiation and would enable new knowledge on aerosol influences on climate to be gained.

An analogy can be drawn between improving knowledge of aerosol-cloud interactions through a limited area perturbation experiment and previous experiments conducted to investigate the control of micronutrients (notably iron) on the drawdown of carbon by marine biological systems. A number of experiments have been conducted which have deliberately added iron to the ocean to improve knowledge of ocean biological carbon cycling. These have substantially improved knowledge of nutrient limitation on oceanic primary production, its subsequent control on plankton communities and how this impacts on cycling of carbon and nitrogen in the world's oceans (Boyd et al., 2007). Further fertilization experiments to develop knowledge of the fundamental processes are seen as crucial to furthering understanding of Earth system and are critical before any consideration is given to large scale deliberate attempts at carbon sequestration by such means (Lampitt et al., 2008). A major concern is that larger scale experiments may have significant impacts on ocean ecosystems. A key point is that a limited area field experiment to study aerosol-cloud interactions using artificially generated aerosol from sea spray can be carried without any climatically damaging effects as the lifetime of atmospheric aerosol in the marine boundary layer is of the order of a few days at most. Such experiments therefore offer a valuable contribution to climate science and should not be viewed as solely a means of validating the cloud brightening scheme.

Here we present an initial framework for the testing and implementation of such experiments. We propose a set of field tests to critically assess the efficacy of the marine cloud brightening geoengineering proposal over a limited area. The tests are de minimus with respect to their climate effects. The tests involve three phases, with increasing logistical complexity, each of which is designed to test one or more important components of the cloud brightening scheme. Each involves the introduction and monitoring of controlled aerosol perturbations from one or more ship-based seeding platforms up to a limited area of 100×100 km^2. A suite of observational platforms of increasing number and complexity, including aircraft, ships and satellites, will be required to observe the aerosol plume and in the latter experiments the cloud and albedo responses to the aerosol perturbations, including the necessary cloud physical and chemical processes that determine the efficacy of the cloud brightening scheme and are central to the broader questions of aerosol-cloud interactions. Multi-scale modelling work will be carried out to simulate/predict the cloud responses. The modelling work will be used to drive quantitative hypothesis testing for the field tests, and will be used to test our understanding of, and ability to simulate, aerosol-cloud interactions on the regional scale.

The scale and complexity of such experiments have been delivered by the international research community on several occasions over the last decade. Most recently, the VAMOS (Variation n the American MOnsoon System) Ocean Cloud Atmosphere Land Study (VOCALS) was developed to improve understanding of the South East Pacific coupled ocean-atmosphere-land system on diurnal to inter-annual timescales. A large component of VOCALS centered around a large scale Regional Experiment to investigate the interactions between aerosol, cloud and precipitation across a strong pollution gradient in a region dominated by the largest and most persistent stratocumulus cloud sheet on the planet (Wood et al., 2010). The field experiment involved the use of 5 aircraft and 2 research ships, operating in the region between 70 and 80W at a longitude of around 20S for a period of around 4 to 6 weeks and received multi-agency and multi-national support. Such integrated international collaboration would be necessary to deliver a full limited area field test of aerosol-cloud-precipitation interactions generated by a sea spray generation system.

The recommended approach is to test any sea spray generation method, its effect on the cloud system and subsequent radiative impacts through a series of field trials of increasing complexity. The first phase is to establish the ability of a full size spray generation system to deliver sea spray particles of the correct size and number in such a way that they become mixed throughout the depth of the boundary layer. The second phase would be to utilize a single system to investigate cloud response and the third phase would be to conduct a multi source limited area experiment at the 100 km x 100 km scale. Such a strategy assesses viability at each stage without incurring unnecessary risk or expense.

Field Phase 1 – Injection and dispersion of particles

Technology to create the large number of small particles that can act as cloud condensation nuclei on which cloud droplets will form, will need to be field tested to ensure that the delivery mechanism (here termed injection) can deliver particles in sufficient quantity and of the appropriate size into the marine boundary layer (MBL), and to study the dispersion of the aerosols throughout the MBL.

The seeding technology should be deployed on a ship or barge platform in a marine region favorable for marine cloud brightening. Only a single aircraft fitted with state of the art aerosol measurement technology would need to be deployed to sample the aerosol plume as a function of the distance downwind of the injection source.

This study does not need to be carried out in the remote ocean boundary layer and could be located near to the coast for convenience during the early stages of testing of the engineering system. Studies of diesel-burning commercial shipping indicate that a single source will generate a plume that is typically 10 km wide at a distance of 100 km downwind. The aircraft would be used to examine the physical and chemical characteristics of particles (size distribution, chemical composition, cloud-forming properties) close to the injection source and to examine how these particles disperse in the boundary layer with distance downwind. Tracer technology should be employed to unequivocally identify the plume and hence record if concentrations of sea salt are undetectable from the background. No attempt should be made in Phase 1 to study the cloud responses to the aerosol plume. To do so would significantly increase the complexity of the experiment and would represent a risk were any given generation scheme to fail to deliver the required perturbation. Modelling activities in this phase should focus on examination of the processes associated with the formation of particles and their modification in the stack, and on aspects of the dispersion and mixing of aerosols throughout the boundary layer downwind of the source.

Field Phase 2 – Single source cloud responses

Once the injection and dispersion technology has been tested and the aerosol plume characterized, the next stage is to examine the cloud responses to a single injection source. The cloud response to a single source will be in the form of a ship track (albeit a deliberately produced

one), for which there are existing observations (e.g. the Monterey Area Ship Track Experiment in 1994). Figure 13 shows a schematic of the scale of such a plume.

Measurement of both the aerosol characteristics below the cloud and of the cloud physical processes should be made with multiple aircraft platforms. The goal would be to test the sensitivity of the cloud microphysical properties to the aerosol perturbations in the plume and to contrast these with the surrounding unseeded clouds under a range of conditions. Once again, releasing a tracer from the spray generation system would provide a useful identification of the plume position. Combinations of volatile organic carbon compounds with varying chemical lifetimes can be used to not only identify the plume but also determine its photochemical age and these can be identified online using modern mass spectrometric or online chromatographic methods.

Modelling work would be conducted with both process-scale cloud models and with climate models, to test the cloud microphysical responses. These modelling studies should be used to quantitatively predict the outcome of introducing multiple injection sources, which is the key task in Phase 3 testing

Field Phase 3 – Multiple source limited area experiment

In the third phase of the proposed field trials, multiple (between 5 and 10) injection sources (see figure 13) would be used to create a line (of order 100 km long) of injection sources approximately perpendicular to the mean wind. The plumes from these sources would disperse and will create a single broad perturbed area extending from the source line several hundred km or more downwind. At such scales the changes in the cloud filled boundary layer as a result of the doping by particles should be detectable from space if the radiative impact is significant.

Multiple observational platforms should be used to study (i) the aerosol physical and chemical properties below the cloud inside and outside of the seeded area; (ii) the cloud microphysical, structural and dynamical responses; (iii) the cloud albedo response. Measurements should be made at different distances downwind of the source line. Aircraft flights at stacked levels below cloud, in-cloud, and above cloud would be complemented by a research ship that will continuously sample the air at a variety of distances downwind of the source line. Control experiments could be performed in two ways: (i) *spatial control* would involve contrasting the seeded area with the surrounding region; (ii) *temporal control* would involve temporal modulation of the source strength, perhaps with 6 hour on-off frequency. The required duration of the entire field test will likely be a month or more, which will permit perhaps 15 aircraft case studies under different meteorological conditions and under different background aerosol regimes. Sufficient temporal control modulation would be available on these timescales to provide adequate constraints for model studies.

The albedo response to the aerosol perturbations would be quantitatively determined using a combination of airborne and satellite remote sensing. One of the research aircraft would be dedicated to remote sensing measurement of the radiation field above the clouds. Process-scale and climate modelling should be performed to quantitatively test the marine cloud brightening hypothesis. This should involve studies designed to calculate the expected magnitude of the albedo perturbations as a function of the seeding strength and meteorological conditions and to compare these with the observations.

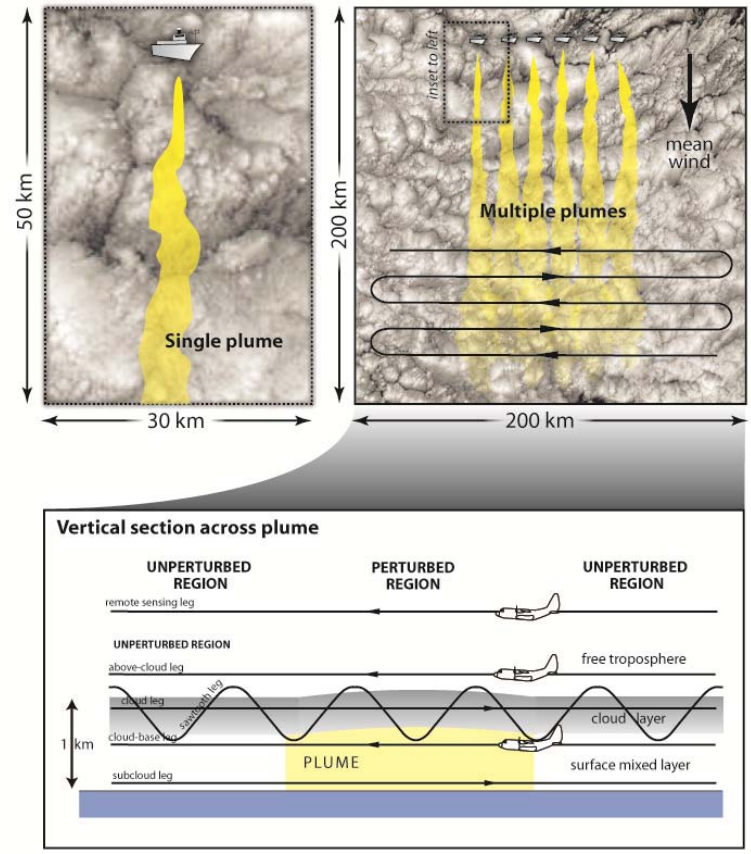

Figure 13 *A schematic of the plumes and the field experiment design*

7.. **Discussion**

It is unclear whether deployment of the cloud MCB geoengineering technique would ever be warranted, should the climate-change problem reach such a drastic stage that some form of intervention seemed required. GCM modeling by three independent groups, using three different models, (Jones et al. (2009), Rasch et al. (2009) and Bala et al, (2010)) indicates that if it functioned as assumed in the modelling, it could stabilize the Earth's average surface temperature and maintain current levels of polar sea-ice cover at approximately current values for some decades, at least up to the CO2-doubling point, where the required negative forcing is about -3.7 W/m2. However, as discussed in Section 4, marine stratocumulus clouds are much more complex than has been implicitly assumed in this modeling, and much more fundamental research into these clouds is required before we can establish whether our assumptions are justified to an acceptable degree. Also, we have not yet established – for all situations of interest - quantitative values for the fraction of spray droplets generated at or near the ocean surface, which enter the bases of the clouds above. Nor have we succeeded to date in developing a seawater spray production system that meets our requirements as to droplet size and spray-rate. Finally, we have not yet thoroughly examined the (possibly adverse) ramifications of the deployment of the technique. No case for deployment would exist unless it was established that all unacceptable ramifications could be remedied.

Two advantages of MCB, in principle, are that: (1) the sprays could be switched off immediately, with essentially all of the seawater droplets returning to the ocean within a few days: (2), since, for some decades, not all suitable clouds would need be seeded in order to produce sufficient negative forcing to balance the CO2-increase, there exists – in principle - flexibility to confine the seeding to selected cloudy areas which eliminate adverse consequences or reduce them to acceptable limits.

If MCB proves to be viable, and deployment of an SRM scheme necessary, optimal beneficial cooling might be produced, if it was utilized in concert with another hopefully viable technique (e.g. stratospheric sulphur seeding, Crutzen (2006), or micro-bubble ocean whitening, Sietz, (2010)). In the former case, for example, the primary cooling could be supplied by the stratospheric scheme, with beneficial adjustments being made by cloud brightening, which can function in a more localized manner. It may even prove useful to produce localised warming via seeding, to optimize this fine tuning.

Other issues which might be addressed by exploiting the localized initial cooling produced by MCB, (and/or the micro-bubble technique), are coral reef protection and hurricane emasculation. In the latter case, it may prove possible to cool oceanic waters in the regions where hurricanes spawn. This would probably require continuous seeding over several months, culminating in the hurricane season. Also, it may prove possible to produce sufficient polar cooling to maintain existing sea-ice cover by seeding specially selected cloudy regions of much smaller total area than considered by Rasch et al. (2009).

Bala et al. (2010) found that when MCB was employed in a CO2-doubled environment the cooling associated with cloud seeding was a maximum in the two polar regions, compensating closely for the preferential warming resulting from the additional carbon dioxide. Our own modelling (Section 2) produced similar results. Irvine et al. (2010) point out that such compensation does not occur as a consequence of utilization of the large-scale SRM techniques [stratospheric sulphate aerosol injection (Crutzen, 2006) or solar “sunshade” (Angel, 2006)]. They also concluded from their modelling that it might be possible to identify a level of SRM geoengineering capable of simultaneously meeting more than one target, such as maintaining a stable mass balance of the Greenland ice sheet without exposing significant fractions of the Earth to “novel” climate conditions.

A comprehensive series of model inter-comparisons is urgently required in order to optimize and better quantify our understanding and assessment of MCB. We stress again that to optimize our understanding of this geoengineering technique, we must conduct a parallel programme of fundamental research into the associated cloud physics and chemistry, aerosol properties and transport, meteorology, etc.

If satisfactory resolution of all significant problems associated with MCB, identified earlier, were to be achieved, and a need for its deployment was deemed to exist, it would be necessary to make an informed decision as to the type of vessel to be used for spray dissemination. Seeding from aircraft is one possibility. Salter et al. (2008) focused attention on wind-powered, unmanned, satellite guided Flettner ships, and it was estimated that about 1500 spray-vessels, each consuming about 150KW (derived from the wind) would be required to produce the globally averaged negative forcing of -3.7 W/m2 required to balance CO2-doubling. A conventional powered ship might consume about 1MW, so for both types of vessel the ratio of the rate of planetary radiative loss to required operational power is huge (in the range 10**5 to 10**7). It follows that considerations of energy efficiency, desirable though that is, should not dictate the selection of type of spray vessel. Latham et al. (2008) pointed out that the main reason this ratio is so high for MCB is that Nature provides the energy required for the increase of surface area of newly activated cloud droplets by 4 or 5 orders of magnitude as they ascend to cloud top and reflect sunlight.

The above arguments are based on the assumption that current GCM modeling is reasonably accurate. However, if it transpires that estimated albedo-change / droplet flux ratio values are seriously inflated because, for example, of significant over-estimation of the fraction of disseminated seawater particles which rise into the clouds, this issue would need to be re-assessed. Other factors then to consider include the levels of pollution produced by spray vessels and the energy they consume. In principle, nuclear-powered vessels could be utilized. It is also to be noted that during the decades leading to CO2-doubling, the amount of negative forcing required of MCB will be correspondingly less, as will the emissions (which would of course be zero for wind-powered vessels). Definitive statements on these issues must wait on further research.

Acknowledgements.

Funding for elements of this research was provided by the Fund for Innovative Climate and Energy Research, FICER, at the University of Calgary. This does not constitute endorsement of deployment in any form of Cloud Albedo Modification by the funding agency. Part of this work was performed at the Stanford Nanofabrication Facility, supported by National Science Foundation Grant ECS-9731293. We are grateful to Graham Feingold for helpful comments.

References.

Abel, S. J., Walters, D. N., and Allen, G. 2010: Evaluation of stratocumulus cloud prediction in the Met Office forecast model during VOCALS-Rex, *Atmos. Chem. Phys. Discuss.*, **10**, 16797–16835,

Ackerman, A. S., Kirkpatrick, M. P., Stevens, D. E., and Toon, O. B. 2004 The impact of humidity above stratiform clouds on indirect aerosol climate forcing, *Nature*, **432**, 1014–1017, (DOI 10.1038/nature03174.)

Ackerman, A. S., Coauthors 2009: Large-eddy simulations of a drizzling, stratocumulus-topped marine boundary layer. *Mon. Wea. Rev.*, **137**:1083–1110.

Albrecht, B. 1989 Aerosols, cloud microphysics, and fractional cloudiness, *Science*, **245**, 1227–1230,

Angel, R. 2006. Feasibility of cooling the Earth with a cloud of small spacecraft near the inner Lagrange point (L1). Proc. Natl. Acad. Sci.103 (46) 17,184-17,189. doi:101073/pnas.0608163103.

Bala G., Caldreia K., Nemani R., Cao L., Ban-Weiss G. and Shin H-J. 2010 Albedo enhancement of marine cloud to counteract global warming: impacts on the hydrological cycle. *Clim Dynam* (DOI 10.1007/s00382-010-0868-1)

Bennartz, R. 2007. Global assessment of marine boundary layer cloud droplet number concentration from satellite. *J Geophys Res-Atmos*, **112(D2)**, D02201

Bocanegra, R., Galán, D., Márquez, M., Loscertales, I. G. & Barrero, A. 2005 Multiple electrosprays emitted from an array of holes. *J. Aerosol Sci*. **36**, 1387–1399. (DOI:10.1016/j.jaerosci.2005.04.003)

Bony, S. and Dufresne, J. -L. 2005 Marine boundary layer clouds at the heart of tropical cloud feedback uncertainties in climate models*, Geophys. Res. Lett*., **32**, L20806, (DOI:10.1029/2005GL023851.)

Bower, K., K, T. Choularton, J. Latham, J. Sahraei, S. Salter, 2006, Computational assessment of a proposed technique for global warming mitigation via albedo enhancement of marine stratocumulus clouds*, Atmos. Res*.**82**, 328-336

Boyd, P. W., Jickells,T., Law, C. S., Blain, S., Boyle, E. A., Buesseler, K. O., Coale, K. H., Cullen, J. J., de Baar, H. J. W., Follows, et al. 2007 Mesoscale Iron Enrichment Experiments 1993-2005: Synthesis and Future Directions, *Science*, **315**. no. 5812, pp. 612 – 617, (DOI: 10.1126/science.1131669)

Bretherton,C. S., P. N. Blossey and J. Uchida 2007: Cloud droplet sedimentation, entrainment efficiency, and subtropical stratocumulus albedo, *Geophys. Res. Lett.*, **34**, L03813, doi:10.1029/2006GL027648

Bretherton, C. S., Wood, R., George, R. C., Leon, D., Allen, G., and X. Zheng, 2010: Southeast Pacific stratocumulus clouds, precipitation and boundary layer structure sampled along 20 S during VOCALS-REx, *Atmos. Chem. Phys. Discuss.*, **10**, 15921-15962.

Byun, D., Lee, Y., Tran, S. B .Q., Nugyen, V. D., Lee, S., Kim, S., Inamdar, N., Park, B. & Bau H. 2008 Electrospray on super hydrophobic nozzles treated with argon and oxygen plasma. *Appl. Phys. Lett.* **92**, 093507. (DOI:10.1063/1.2840725)

Connolly P,, O. Möhler, P. R. Field, H. Saathoff, R. Burgess, T. Choularton, and M. Gallagher, 2009, Studies of heterogeneous freezing by three different desert dust samples*, Atmos. Chem. Phys*., **9**, 2805-2824.

Craft, T. J., Gerasimov, A. V., Iacovides, H. and Launder, B. E., 2004, The negatively buoyant wall jet: The performance of options in RANS modelling, *Int. J. Heat Fluid Flow* **25**, 809-823.

Craft, T. J. Iacovides, H. and Launder, B. E., 2010, Computational modelling of Flettner rotor performance with and without Thom discs, Proc. 7th Conference on Engineering Turbulence Modelling & Measurements, 152-157, Marseilles, June 2010.

Crowley, J. M. 1977 Role of Joule heating in the electrostatic spraying of liquids. *J. Appl. Phys*. **48**, 145–147. (DOI:10.1063/1.323299)

Crutzen, P. J. 2006 Albedo enhancement by stratospheric sulfur injections: A contribution to resolve a policy dilemma, *Climatic Change,* **77**, Issue: 3-4, pp. 211-219

De la Mora, J. F. 2007 The fluid dynamics of Taylor cones. *Ann. Rev. Fluid Mech*. **39** 217–243.

Deng, W., Waits, C. M., Morgan, B. & Gomez, A. 2009 Compact multiplexing of monodisperse electrosprays. *J. Aerosol Sci*. **40** 907–918. (DOI:10.1016/j.jaerosci.2009.07.002)

DPSS Lasers Inc, 2525 Walsh Ave., Santa Clara, CA 95051 USA.

Feingold, G., I. Koren, H. Wang, H. Xue, and W. A. Brewer, 2010: Precipitation-generated oscillations in open cellular cloud fields, *Nature*, **466**, 849-852. (DOI:10.1038/nature09314)

Gañán-Calvo, A. M. & Montanero, J. M. 2009 Revision of capillary cone-jet physics: Electrospray and flow focusing. *Phys. Rev. E* **79**, 066305 and 069905. (DOI:10.1103/PhysRevE.79.066305) and (DOI:10.1103/PhysRevE.79.069905)

IPCC 2007 In Climate change 2007: the physical science basis. *Contribution of working group to the fourth assessment report of the intergovernmental panel on climate change* (eds S. Solomon, D. Qin, M. Manning, Z. Chen, M. Marquis, K. B. Averyt, M. Tignor & H. L. Miller). Cambridge, UK: Cambridge University Press.

Irvine, P.J.A.Ridgwell & D.J. Lunt (2010),Assessing the regional disparities in geoengineering impacts. *Geophys. Res. Lett*. 37, L18702. doi:10.1029/2010GL044447..

Jacobson, M. 2005: *Fundamentals of Atmosphericmodelling, 2nd ed*. Cambridge University Press, New York

Johnson, D. W., Osborne, S., Wood, R., Suhre, K., Quinn, P. K., Bates, T., Andreae, M. O., Noone, K. J., Glantz, P., Bandy, et al 2000 Observations of the evolution of the aerosol, cloud and boundary-layer characteristics during the 1st ACE-2 Lagrangian experiment, *Tellus*, **52B**, pp. 348–374,

Jones A., Hayward J. and Boucher O., 2009: Climate impacts of geoengineering marine stratocumulus clouds. *J Geophys Res*.**114** D10106

Jones A., Hayward J. and Boucher O., 2010: A comparison of the climate impacts of geoengineering by stratospheric SO2 injection and by brightening of marine stratocumulus clouds. *Atmos. Sci. Lett.*

*Korhonen H. , Carslaw K. S. And Romakkaniemi S. 2010 Enhancement of marine cloud albedo via controlled sea spray injections: a global model study of the influence of emission rates, microphysics and transport. Atmos. Chem. Phys. Discuss., **10**, 735-761*

Kubar, T.L., D. L. Hartmann, and R. Wood, 2009: Understanding the Importance of Microphysics and Macrophysics for Warm Rain in Marine Low Clouds - Part I. Satellite Observations, *J. Atmos. Sci*., **66**, 2953-2972.

*Lampitt, R. S., Achterberg, E. P., Anderson, T. R., Hughes, J. A., Iglesius-Rodriguez, M. D., Kelly-Gerreyn, B. A., Lucas, M., Popova, E. E., Sanders, R., Shepherd, J. G. et al 2008. Ocean fertilization: a potential means of geoengineering?, Phil. Trans. R. Soc. A **366**, 3919–3945 (DOI:10.1098/rsta.2008.0139)*

Latham, J. 1990 Control of global warming? *Nature* **347**, 339-340. (DOI:10.1038/347339b0)

Latham, J. 2002 Amelioration of global warming by controlled enhancement of the albedo and longevity of low-level maritime clouds. *Atmos. Sci. Lett*. **3**, 52-58. (DOI:10.1006/Asle.2002.0048)

Latham, J., Rasch, P., Chen, C.-C., Kettles, L., Gadian, A., Gettelman, A., Morrison, H., Bower, K. and Choularton, T. 2008. Global temperature stabilization via controlled albedo enhancement of low-level maritime clouds, *Phil. Trans. R. Soc. A* **366** (1882): 3969–3987.

Leon D. C., Z. Wang, and D. Liu 2008: Climatology of drizzle in marine boundary layer clouds based on 1 year of data from CloudSat and Cloud-Aerosol Lidar and Infrared Pathfinder Satellite Observations (CALIPSO), *J. Geophys. Res.*, **113**, D00A14.

Lien, F-S and Leschziner, M. A., 1994 A general non-orthogonal finite-volume algorithm for turbulent flow at all speeds incorporating second-moment closure. Part 1: Numerical implementation, *Comp. Meth. Appl. Mech & Eng'ng* **114**, 123-148.

Lohmann, U., and Feichter, J., 2005: Global indirect aerosol effects: a review. *Atmos. Chem. Phys. **5** 715-737*

Lozano, P., Martínez-Sánchez, M. & Lopez-Urdiales, J. M. 2004 Electrospray emission from non-wetting flat dielectric surfaces. *J. Coll. Inter. Sci*. **276** 392–399. (DOI:10.1016/j.jcis.2004.04.017)

Martin, G., Dearden, C., Greeves, C., Hinton, T., Inness, P., James, P., Pope, V., Ringer, M., Slingo, J., Stratton, R. and Yang G-Y., 2004: Evaluation of the atmospheric performance of HadGAM/GEM1: Hadley Centre technical note 54

McCormick M. P., Thomason, L. W., and Trepte, C. R. 1995 Atmospheric effects of the Mt Pinatubo eruption., *Nature*, **373**, 399-404

Minnis,P., Harrison, E. F., Stowe, L. L., Gibson, G. G., Denn, F. M., Doelling, D. R., and Smith, Jr. W. L. 1993 Radiative Climate Forcing by the Mount Pinatubo Eruption, *Science*, **259**, 1411-1415,

Mittal, S. and Kumar, B., 2003, Flow past a rotating cylinder, *J. Fluid Mech.*, **476**, 302-334.

Rasch P., Latham J. and Chen C-C. 2009: Geoengineering by cloud seeding: influence on sea ice and climate system. *Environ*. *Res*. *Lett*, **4**, 045112

Reid, E. G., 1924, Tests of rotating cylinders, NACA-TN-209

Repellix™: Integrated Surface Technologies, Inc., 1455 Adams Dr., Menlo Park, CA 94025 USA

Reverchon, E. & Spada, A. 2004 Crystalline micro-particles of controlled size produced by super-critical atomization. *Ind. Eng. Chem. Res*. **43**, 1460–1465. (DOI:10.1021/ie034111t)

Robock, A., Bunzl, M., Kravitz, B., Georgiy L. Stenchikov, G. L. 2010 A Test for Geoengineering? *Science*, **327**. no. 5965, pp. 530 – 531 (DOI: 10.1126/science.1186237)

Rosenfeld, D., Y. J. Kaufman, and I. Koren, 2006: Switching cloud cover and dynamical regimes from open to closed Benard cells in response to the suppression of precipitation by aerosols. Atmos. Chem. Phys., 6, 2503–2511.

Russell, L. M., Seinfeld, J. H., Flagan, R. C., Ferek, R. J., Hegg, D. A., Hobbs, P. V., Wobrock, W., Flossmann, A., O'Dowd, C. D., Nielsen, K. E. et al 1999 Aerosol dynamics in ship tracks, *J. Geophys. Res.*,**104** pp 31,077-31,095

Salter, S., Sortino, G. and Latham, J., 2008, Sea-going hardware for the cloud-albedo method of reversing global warming, *Phil. Trans. Roy. Soc.*, **366**, 3843-3862

Seinfeld J. and S. Pandis, 2006, *Atmospheric Chemistry and Physics: From air pollution to climate change, 2nd ed*, Wiley.

Sietz, R, 2010 *Climatic Change*: Bright Water:Hydrosols, Water Conservation and Climate Change. Accepted

Stevens, B., and Feingold, G. 2009 Untangling aerosol effects on clouds and precipitation in a buffered system, *Nature*, **461**, (DOI:10.1038/nature08281.

Stevens, B., Lenschow, D. H., Vali, G., Gerber, H., Bandy, A., Blomquist, B., Brenguier, J.-L., Bretherton, C. S., Burnet, F., Campos., T., et al 2003 Dynamics and chemistry of marine stratocumulus – DYCOMS II, *Bulletin Am. Meteorol. Soc.*, 579-593, (DOI: 10.1175/BAMS-84-5-579.)

Taylor, G. 1964 Disintegration of water drops in an electric field. *Proc. Roy. Soc. A* **280**, 383–397. (DOI:10.1098/rspa.1964.0151)

Thom, A., 1934, Effects of discs on the air forces on a rotating cylinder, *Aero. Res. Council R&M* **1623**.

Topping D., G. B. McFiggans, and H. Coe, 2005, A curved multi-component aerosol hygroscopicity model framework: Part 1 – Inorganic compounds, *Atmos. Chem. Phys*, **5**, 1205-1222

Twomey, S. 1974 Pollution and the planetary albedo, *Atmos. Environ*., **8**, 1251–1256

Twomey, S. 1977 Influence of pollution on the short-wave albedo of clouds. *J. Atmos. Sci.,* **34,** 1149-1152

Wang, H., and G. Feingold, 2009a:modelling open cellular structures and drizzle in marine stratocumulus. Part I: Impact of drizzle on the formation and evolution of open cells. *J. Atmos. Sci.*, **66**, 3237-3256.

Wang, H., and G. Feingold, 2009b:modelling open cellular structures and drizzle in marine stratocumulus. Part II: The microphysics and dynamics of the boundary region between open and closed cells. *J. Atmos. Sci.*, **66**, 3257-3275.

Wang, H., P. J. Rasch, and G. Feingold, 2010: A process-modeling study of aerosol-cloud-precipitation interactions in response to controlled seawater spray, in preparation.

Wang, S. P.,Wang, Q., and Feingold, G. 2003 Turbulence, condensation, and liquid water transport in numerically simulated nonprecipitating stratocumulus clouds, *J. Atmos. Sci.*, **60**, 262–278.

Wood, R. 2007 Cancellation of aerosol indirect effects in marine stratocumulus through cloud thinning, *J. Atmos. Sci.*, **64**, 2657–2669, (DOI:10.1175/jas3942.1)

Wood, R., Bretherton, C. S., Leon, D., Clarke, A. D., Zuidema, P., Allen, G., and Coe, H. 2010 An aircraft case study of the spatial transition from closed to open mesoscale cellular convection, *Atmos. Chem. Phys. Discuss.*, in review,

Wyant, M. C., Wood, R., Bretherton, C. S., Mechoso, C. R., Bacmeister, J., Balmaseda, M. A., Barrett, B., Codron, F., Earnshaw, P., Fast, J. et al 1997 Global precipitation: A 17-year monthly analysis based on gauge observations, satellite estimates, and numerical model outputs. 2010 *Bull. Amer. Meteor. Soc.*, **78**, 2539 - 2558.

Xie, P., and P.A. Arkin, 1997: Global precipitation: A 17-year monthly analysis based on gauge observations, satellite estimates, and numerical model outputs. *Bull. Amer. Meteor. Soc.,* **78**, 2539 - 2558.

Zeleny, J. 1917 Instability of electrified liquid surfaces, *Phys. Rev*. **10**, 1–6. (DOI:10.1103/PhysRev.10.1)